**This is the Preprint Version.**

Mhd Anwar Orabi, Aatif Ali Khan, Liming Jiang, Tejeswar Yarlagadda, Jose Torero, Asif Usmani, Integrated nonlinear structural simulation of composite buildings in fire, Engineering Structures, 2021, https://doi.org/10.1016/j.engstruct.2021.113593.

# Integrated Nonlinear Structural Simulation of Composite Buildings in Fire

**Mhd Anwar Orabi[1], Aatif Ali Khan[1,*], Liming Jiang[1] , Tejeswar Yarlagadda[1], Jose Torero[2], Asif Usmani[1]**

*[1]Department of Building Services Engineering, The Hong Kong Polytechnic University, Hong Kong*

*[2]Department of Civil, Environmental & Geomatic Engineering, University College London, London, UK*

## ABSTRACT

The collapse of several tall composite buildings over the last two decades has shown that the performance of tall, composite and complex buildings in fire is a necessary design consideration that ought to go beyond simple code compliance. To this end, several advancements in the field of numerical simulation of both the fire and the thermomechanical response of structures have been made. In isolation, the practical benefit of these advancements is limited, and their true potential is only unlocked when the results of those numerical simulations are integrated. This paper starts by showcasing recent developments in the thermal and thermomechanical analysis of structures using OpenSees. Integration of these developments into a unified simulation environment combining fire simulation, heat transfer, and mechanical analysis is then introduced. Finally, a demonstration example based on the large compartment Cardington test is used to showcase the necessity and efficiency of the developed simulation environment for thermomechanical simulation of composite structures in fire.

**Keywords** –complex building, tall building, CFD, coupling, resilience

## 1. Introduction

Modern architectural designs seek to maximise open space within a building, allow for natural light, and improve thermal comfort using natural ventilation and heavily insulated building envelopes. This is particularly the case for office buildings where tenants occupy large areas. These aims produce a more environmentally and occupant friendly built environment, but also introduce a set of hidden but serious fire hazards. Thermally efficient cladding systems, for example, were amongst the factors that led to the tragic and deadly Grenfell Tower disaster [1,2]. The risks posed by these systems are often not fully mitigated, and the resulting fires may grow and spread in uncontrollable ways [3]. Another hidden risk arises from the large open spaces that almost completely alter the fire behaviour from the well-established small-compartment-focused standard and parametric temperature-time curves [4,5]. In addition to the life hazard these fires present, the risk for structural collapse also increases because of the often unanticipated severe and complex thermo-mechanical response of the structural system [6].

As the last line of defence against fire, structural fire resilience is of the utmost importance. As the National Institute of Standards and Technology (NIST) concluded from their investigation of the World Trade Center catastrophe: “fire resistance of structures be enhanced by requiring a performance objective that uncontrolled building fires result in burnout without partial or global (total) collapse.” [7]. If this objective is to be met and if composite and complex buildings are to be designed for performance in fire rather than simple code-compliance, then it is necessary to utilise the advanced numerical simulation tools now available [8].

The simulation of structures in fire have progressed in two natural ways: simulation of the fire event,

and simulation of the structural response to that event. For the first, computational fluid dynamics (CFD) analysis has emerged as the most prevalent method. Currently, there are many available CFD tools capable of simulating fire behaviour such as OpenFOAM, CFX, and fire dynamics simulator (FDS). FDS is an open-source CFD engine written in FORTRAN by NIST and specialising in the simulation of fire and smoke [9]. Despite being the most prevalent and virtually the industry-standard, FDS has some limitations as will be discussed in first section of the article. For the simulation of the structural response to the fire event multiple tools also exist. OpenSees is one of these tools which uses the finite element method (FEM) to analyse structural response [10]. Since OpenSees is an open-source project, it was extended for thermomechanical analysis by researchers first at the university of Edinburgh and currently at the Hong Kong Polytechnic University [11–14]. In addition to its mechanical analysis capabilities, OpenSees also includes a heat transfer (HT) module and material library allowing it to also perform 1D through 3D thermal analyses [15].

While OpenSees is a powerful engine capable of efficiently performing complicated and large simulations, it relies on script input that must be painstakingly written and debugged by the user. Post processing is equally frustrating since there is no built-in way of visualising anything but the simplest results. To mitigate this issue, a general-purpose graphical user interface known as “GiD” was first extended by researchers for the standard version of OpenSees without thermomechanical capabilities [16,17], and then extended by the authors in the course of this work to be used for the simulation of large and complex composite buildings in fire.

While OpenSees for fire has its own library of built-in fire scenarios, there is no built-in way to automatically map temperature results from a CFD analysis to an OpenSees model for simulation of

real fire scenarios, and the user must instead perform this manually one point at a time. Despite the tremendous development in both CFD and FEM modelling methods, the sequential coupling of both models is a challenging task mainly due to the difference in the spatial and temporal resolution of fire and structural domains. Over the last decades, considerable work has been done to couple FEM with CFD models [18–23]. More recent developments have also tackled niche areas such as tunnels [24,25], marine structures [22], and thin metal facades [26]. While these computational tools can allow coupling between fire simulation, thermal and thermomechanical analysis their methods mainly target commercial software such as ANSYS and their codes are limited to small research groups of host institutions and are not open source. This severely limits their usability by the research community and hinders the potential for collaborative development.

This paper aims to fill this gap by linking fire simulation, thermal analysis, and thermomechanical via an open-source integrated simulation environment (ISE). This environment consists of three components: a 3D computer aided design (CAD) model containing information about geometry, an FDS model containing information about the fire, and a GiD model containing information about the HT and thermomechanical response and linking them with each other and with the FDS model. The first section of this paper discusses the background of OpenSees for thermal and thermomechanical analysis and FDS for fire simulation. After that, the implementation ISE is detailed starting with the extended GiD + OpenSees interface, the details of how the various components interact, FDS, and then HT analysis. Finally, a large demonstration example showcasing the efficiency with which the integrated environment enables simulation of composite and complex building structures is presented. It is hoped that with this work researchers and engineers from around the world will be able to tackle

and study significantly more complex and notably larger simulation problems targeting composite and complex buildings in fire. The ISE can be utilised fully by downloading the extended simulation environment and the associated OpenSees version [27,28].

## 2. Background to numerical thermal and thermomechanical analysis capabilities

### *2.1. OpenSees for thermomechanical analysis*

OpenSees has undergone significant enhancements over the last decade to perform thermomechanical analysis. Amongst these, the most recent has been the inclusion of the concrete damage plasticity material (CDP) and nonlinear shell elements for modelling floor slabs [29,30].

The nonlinear layered shell elements sections use a plain stress implementation of the CDP material based on the theory presented in [31,32] and for which the yield surface is shown in Fig. 1 (a). Under biaxial or uniaxial tension, the CDP material can reach at most the tensile strength of the concrete $f_t$. Likewise, it can reach a maximum of the concrete compressive $f_c$ under uniaxial compression, but a higher value in biaxial compression. As the figure shows, this results in the yield surface of the CDP material being the same as the Drucker-Prager in the biaxial compression region but different elsewhere. The evolution of the yield surface is governed by the compressive and tensile fracture energies of the concrete which are idealised as shown in Fig. 1 (b), which relates the tensile and compressive cracking energies $g_t$ and $g_c$ to multiples $n$ and $m$ of the corresponding compressive and tensile yield strain values. Under elevated temperature, the yield surface of the CDP material shrinks as Fig. 1 (a) shows, and the fracture energies are also changed as explained extensively in [29,30].

The reinforcement bars are modelled using the “rebar mesh” approach in which the rebars are represented as a plain stress layer using a uniaxial steel material model. Details about the representation

of the reinforcement bars, and the numerical approach to simulating floors are presented extensively in [29,30].

In addition to the simulation of floors using shell elements, thermomechanical displacement-based elements as well as fibre-based force-deformation cross-section are available with a library of thermomechanical material for the nonlinear simulation of beams and columns [14,33]. The fibre-based cross-section takes a uniaxial material and assigns it to each fibre to allow for the spread of plasticity throughout the section. The plasticity is then interpolated over the Gauss stations of the beam-column element removing the need for the development of discrete hinges and allowing for a finer-grained representation of plasticity. The uniaxial material used for the fibre can be either an elastic-plastic material with isotropic hardening, or the "ECSteel" material model with smooth transition from elastic to plastic state. Both steel materials follow the Eurocode guidelines for thermal degradation and are discussed in more detail in [12].

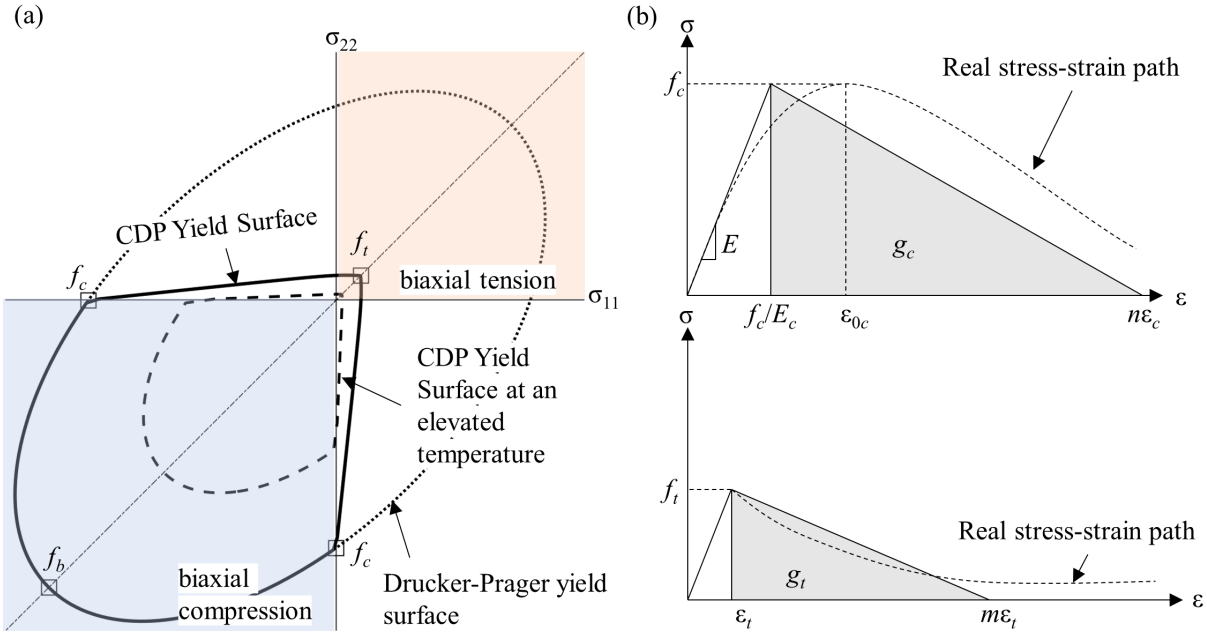


Fig. 1. CDP material definition in OpenSees based on the authors' previous work [29] (a) yield surface, and (b) idealised definition of compressive and tensile fracture energies

Thermal load can be applied to the shell elements at up to nine temperature points across the depth, and up to 15 points across the cross section of a fibre-based beam-column cross section. The number of temperature points across the depth was chosen to accurately capture the nonlinear thermal profiles that develop within floor slabs. The relative location of these points within the section is customisable so that more refinement can be achieved in the heated bottom layers where the temperature profile is most complex. For slab sections with typical dimensions (100 – 300 mm), however, it has been shown elsewhere that 9 evenly-spaced points across the depth are sufficient and so will be used in the demonstration example to follow [11,12]. If customisable temperature point locations are desired by the user, then they would have to simply add this information to the load information in the analysis script before running OpenSees.

One of the major drawbacks to the thermomechanical capabilities of OpenSees is the difficulty involved in model building. As a researcher-developed open-source computational framework, OpenSees relies on script-based input where the user must manually define the nodes, materials, elements, constraints, and loads. Despite this, researchers have previously used OpenSees to build large models and analyse complicated load cases. The process usually relies on full simulation in other software and then like-to-like translation into OpenSees code [34,35], or laborious construction of large scripts using common programming tools [29]. Neither of these approaches is practical, and in the case of the latter there remains many difficulties in visualising large-scale results. This issue is tackled in section 3.1 by the extension of the pre and postprocessor GiD and its OpenSees interface [16,17].

### *2.2. OpenSees for thermal analysis*

In addition to thermomechanical analysis, OpenSees is also capable of performing HT analysis. The

HT and thermomechanical solvers operate on separate domains and can thus be viewed as separate modules. Details of how thermal analysis works within OpenSees can be found in [15]. Similar to thermomechanical analysis within OpenSees, the HT module takes in a script that defines the problem and outputs the results as text files. Since the initial work on the HT module presented in [15] and in [36], several new material definitions were added to the HT module particularly for thermal insulation.

Unlike concrete and steel, it is more difficult to establish temperature-dependent thermal properties for insulation materials. As explained in Kodur and Shakya [37], commercially available insulation material properties are often proprietary, and their temperature-dependent parameters are seldom known. To address this issue, Kodur and Shakya [37] experimentally tested the thermal properties of three spray applied fire resistive materials (SFRM), two of which are commonly used in the industry and the last of which has been gaining popularity recently. All the tested SFRM variants (CAFCO-300, Carboline Type-5MD, and Tyfo WRAFP) were gypsum based, and exhibited significantly different thermal properties that are highly sensitive to temperature, particularly in the 200 °C – 700 °C temperature range. The most important thermal properties for heat transfer in OpenSees, namely thermal capacity and conductivity, were adopted from Kodur and Shakya [37] and the implemented expressions pertaining to their elevated temperature properties are given in Table 1. Here it is important to highlight that the original expression developed by [37] for the CAFCO-300 thermal capacity suffered from discontinuity across its limits since it is based on empirical data. To facilitate computational analysis in OpenSees, these minor discontinuities were marginally smoothed, and the thermal capacity relationship implemented in OpenSees takes the modified form shown in Table 1. In addition to the thermal properties from Kodur and Shakya [37], the material properties from Li et al. [38] for another variant

of the Carboline SFRM are also adopted into OpenSees and are shown in the table. Unlike the temperature-dependent relationships for thermal capacity from [37], the relationship for the Carboline variant used in Choe et al. [38,39] and Li et al. [38] is assumed to not vary with temperature.

The temperature-dependent properties of concrete and steel materials used in the OpenSees HT module follow the recommendations of the relevant Eurocodes such as the EN1993 for steel properties and EN1992 for the properties of normal weight concrete [40,41]. It is worth noting that only thermal properties are required for the materials used in the HT modules and no mechanical properties are necessary as the HT and thermomechanical analyses are decoupled.

Table 1. Thermal properties used for different types of insulation material in OpenSees

| | Thermal conductivity (W/mK) | Thermal capacity (J/kgK) |
|---|---|---|
| CAFCO-300 | $k_t = \begin{cases} 0.0778 - 0.000054T & 20 \le T < 300 \\ -0.08 + 0.000469T & 300 \le T \le 700 \end{cases}$ | $*\ c_p = \begin{cases} 3236 + 5.295T & 20 \le T < 200 \\ 7089 - 13.97T & 200 \le T < 400 \\ 1645 - 0.36T & 400 \le T < 700 \\ 1393 & 700 \le T < 1200 \end{cases}$ |
| Carboline Type-5MD | $k_t = \begin{cases} 0.121 - 0.000319T & 20 \le T < 200 \\ 0.0468 + 0.00005T & 200 \le T \le 700 \end{cases}$ | $c_p = \begin{cases} 1627 + 22.3T & 20 \le T < 100 \\ 4446 - 5.05T & 100 \le T < 400 \\ -1336 + 9.37T & 400 \le T \le 700 \end{cases}$ |
| Tyfo WR-AFP | $k_t = \begin{cases} 0.207 - 0.000318T & 20 \le T < 200 \\ 0.147 - 0.000035T & 200 \le T < 400 \\ 0.0054 + 0.000321T & 400 \le T \le 700 \end{cases}$ | $c_p = \begin{cases} 643 + 1.93T & 20 \le T < 200 \\ 1241 - 0.924T & 200 \le T < 400 \\ 195 + 1.71T & 400 \le T < 600 \\ 1826 - 1.08T & 600 \le T \le 700 \end{cases}$ |
| Carboline, [38] | $k_t = \begin{cases} 0.11 + 0.00028T & 20 \le T < 750 \\ 0.32 & 750 \le T \le 1200 \end{cases}$ | $c_p = 1111$ |

*modified expression for continuity

### *2.3. Simulating fire with FDS*

FDS is a powerful CFD software package for fire simulation that was developed by NIST [42]. By solving the equations of conservation of energy, mass and momentum and associated chemical kinetics to model combustion reaction FDS is capable of realistically simulating the behaviour of fire and smoke

[42]. This ability made FDS the simulation package of choice for studying the fires of the World Trade Center buildings 1, 2, and 7 [7,43,44], as well as the recommended fire simulation engine for the proposed ISE presented in this paper.

Fire simulation deals mostly with turbulent flow which FDS solves using the large eddy simulation (LES) approach. In the LES approach, the energy and momentum are solved numerically only for eddies larger than the size of a single cell. For eddies that fall within the mesh size, energy and momentum are modelled approximately leading to FDS being very sensitive to the size of the mesh [45]. While there are a few theoretical methods to estimate a reasonable mesh size [46,47], for practical problems the authors recommend relying on numerical mesh sensitivity testing such as tracking the variation of gas temperatures for different mesh sizes. In addition to the mesh size, parameters such as ventilation conditions, fuel location, chemical properties of combustibles, and even atmospheric conditions can result in the fire simulation deviating from the real modelled event [48]. Furthermore, even with tremendous development in modelling techniques over the last few decades, state-of-the-art fire models are still unable to simulate the gas-phase combustion reactions and complex pyrolysis and phase-change processes of solid fuels.

Because of these complexities and the strong dependency on mesh size, FDS problems and CFD problems in general are often large and very computationally expensive. Therefore, if the ISE is to be practically useful then the FDS model must be made independent from the rest of the ISE such that changes in its other parts such the FEM mesh would not require changing the FDS mesh or rerunning the CFD analysis. This is achieved in the current work by utilising a “thermocouple” entity and making the linking between the FDS and FEM models unidirectional as will be discussed in more detail in

section 3.3.

## 3. The integrated simulation environment and its implementation

### *3.1. The Extended GiD+OpenSees interface*

GiD is a general purpose pre and post processor equipped with a modifiable codebase and a graphical user interface [17]. It has been used by researchers from the Aristotle University of Thessaloniki to develop an open-source graphical user pre and post processor interface for OpenSees [16]. This interface has then been extended by the authors in this work to perform three important tasks:

1. Provide a graphical user-interface for building large OpenSees thermomechanical models.
2. Serve as the centralised core of the ISE by supervising the FDS and HT links.
3. Postprocess thermal and thermomechanical results such as temperatures, thermal elongations, and concrete damage.

For the first task, GiD+OpenSees was extended with the thermomechanical sections as shown in Fig. 2 (a), material, elements, and prescribed thermal load as in Fig. 2 (b). The section interface only requires section dimensions and degree of refinement, and the corresponding OpenSees section discretization is automatically applied within the OpenSees script generated. Likewise, the interface developed in this work for slab modelling asks the user to select the concrete compressive and tensile strengths, the strain corresponding to its compressive strength ($\varepsilon_{0c}$ in Fig. 1 (b)), and the strain multiplier $n$ and $m$. The concrete modulus is automatically calculated using $E = 1.5f_c/\varepsilon_{0c}$ which was shown to be a good approximation as discussed in [29], and the corresponding slab sections are created and assigned. More importantly, the extended GiD+OpenSees interface allows for both manual and automatic thermal loading. The manual thermal loading uses a very simple interface which takes either

a linear temperature profile, as shown in Fig. 2 (b), or a temperature history for a more detailed thermal profile application.

Automatic thermal load application is performed by coupling with FDS using 'thermocouples'. Thermocouples are an abstraction that refer to a point at which temperatures are retrieved from FDS results, heat transfer is performed, and then thermal load is applied for thermomechanical analysis. The 'Thermocouples' interface seen in Fig. 2 (c) allows the user to create a thermocouple for beams, columns, slabs, and composite sections. The thermocouples are assigned to geometrical surfaces and lines, allowing the analyst to have control over their number and location by choosing the divisions of the GiD geometric entities before meshing. The interaction between the thermocouples and the FDS model is discussed in Section 3.3. Fig. 2 (d) and (e) demonstrates how GiD+OpenSees has also been extended with additional functionality to display thermomechanical analysis results such as temperatures , concrete damage, and thermal elongation of reinforcement bars.

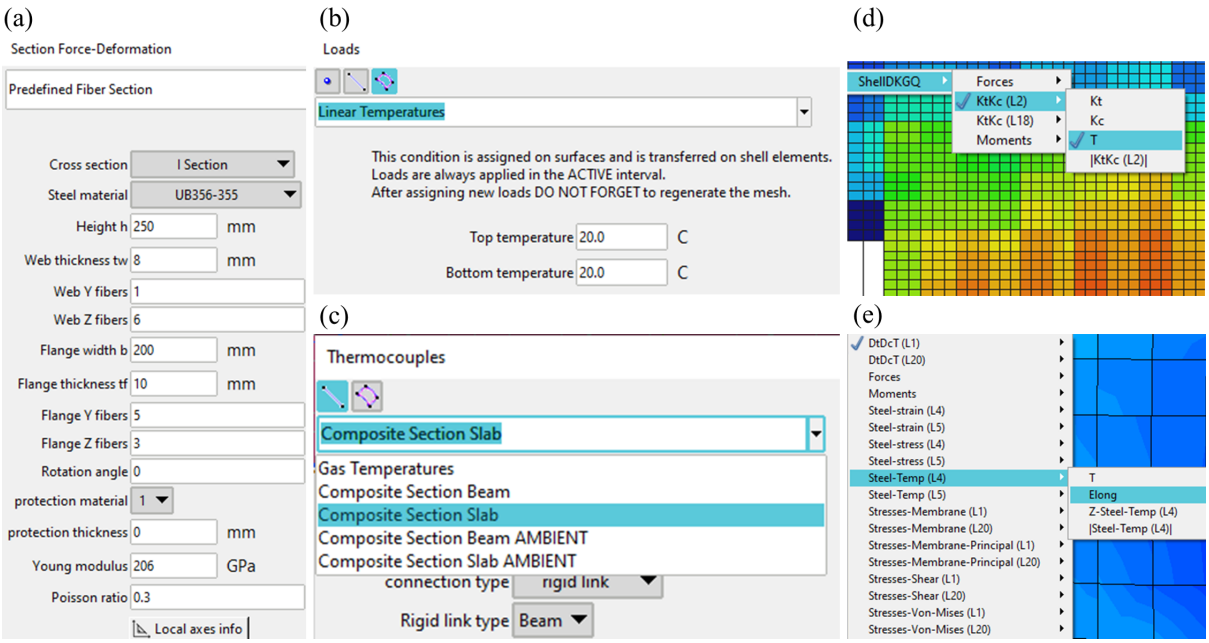


Fig. 2. The extended GiD + OpenSees interface components developed as part of this work (a) thermomechanical fibre section definition interface, (b) assignment of direct thermal load, (c)

definition of thermocouples and composite section connectivity, (d) post processing concrete results and (e) post processing steel bar thermal elongations and temperatures

In addition to the creation of regular thermomechanical materials, sections and elements and the application of thermal loads with a link to FDS results, the developed interface also includes the ability to perform 'smart' composite beam connectivity. The conditions "Composite Section Beam" and "Composite Section Slab" are available from the thermocouple window shown in Fig. 2 (c), and both can be applied to GiD geometric line entities as shown in Fig. 3. The composite section and slab are shown in Fig. 3 (a) and are converted to GiD geometry objects in Fig. 3 (b), and then meshed in Fig. 3 (c). Note that the 'concrete flange' of the composite beam is abstracted as two surfaces as shown in Fig. 3 (b). The first condition is applied to the steel beam of the composite section, while the second is applied to the line dividing the two surfaces of the top 'concrete flange' of the composite beam. The surfaces divided by the line assigned the "Composite Section Slab" condition will become the concrete top flange of the composite beam during heat transfer and thermomechanical analysis. After the mesh is generated, which is illustrated in Fig. 3 (c), the nodes of the shell elements above the nodes of the beam-column element will have their degrees of freedom linked using one of the following user-selected connectivity methods:

(a) Rigid links that are either:

   i. Beam type: constrains all translations and rotations in addition to P-δ effects

   ii. Bar type: constrains only translational freedoms

(b) Equal degree of freedom: connect only the user-specified freedoms ignoring P-δ effects

(c) Common nodes: for slabs and beams defined without offset and on the same elevation; merges the beam and shell element nodes thus connecting all degrees of freedom

(d) Finite constraint: currently allows the user to use a beam element to represent shear connectors. Corresponding beam elements are created during meshing at each connected node

The method of connectivity is chosen by the user, but the linking is performed automatically by the interface. Each set of two surfaces and one line joined in this way constitute a composite beam unit, and the thermal load applied to them will depend on the HT results of a composite section type as will be discussed in Section 3.4.1.

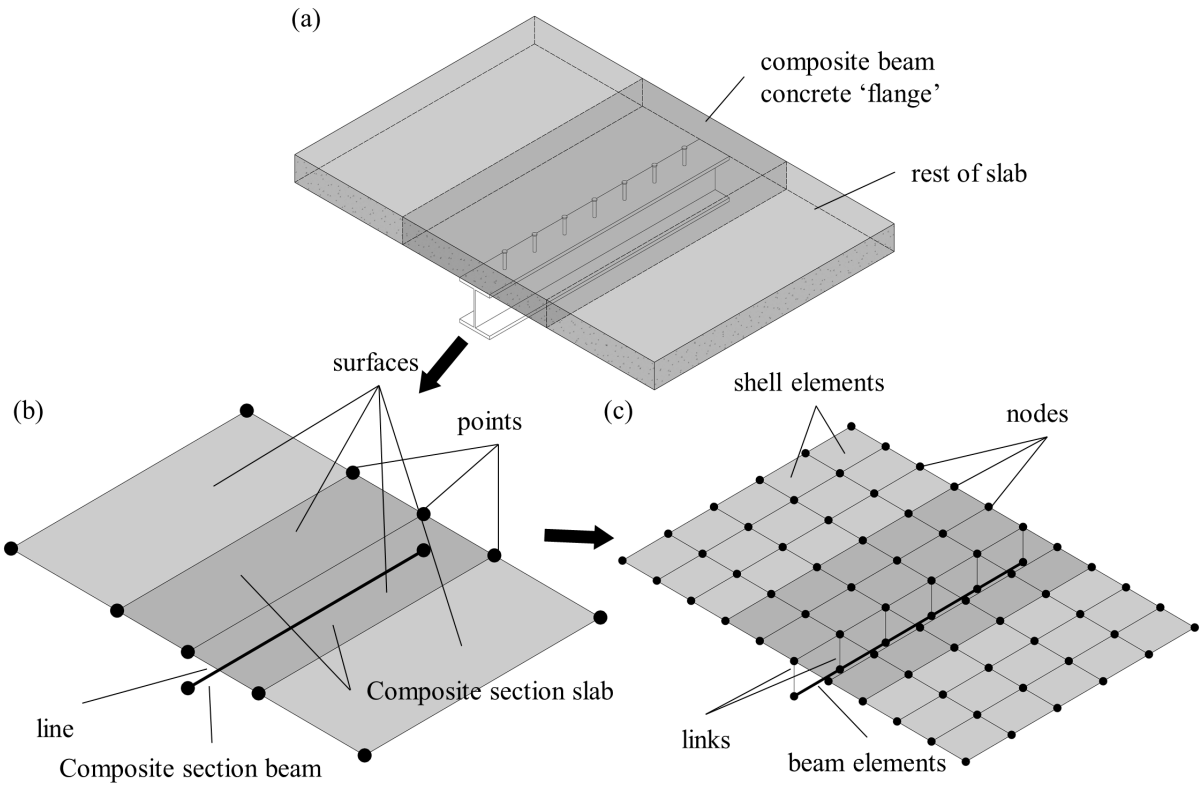


Fig. 3. 'Smart' composite beam connectivity and thermal loading introduced by the ISE (a) section being abstracted into GiD geometry (b) applying "composite section" conditions over the geometry, and (c) automatic connectivity and thermal loading over the mesh

### *3.2. Workflow and component interfacing*

The ISE is a collection of interconnected components for the efficient analysis of large and complex structures in fire. It is made to be simple and adaptable to the workflow of multi-disciplinary engineering teams that aim to tackle complicated structural fire problems. The ISE connects:

1. A CAD model built in Revit or other 3D CAD software.
2. An OpenSees FEM model built in GiD for structural analysis.
3. An FDS model for CFD analysis.
4. Automatic heat transfer performed in OpenSees via a parallel simulation tool.

Cantered around the extended GiD+OpenSees interface discussed in the previous section, the ISE starts off by importing a 3D CAD model into GiD and into FDS. In modern design practices for complex structures, it is expected that a 3D CAD building model is one of the design deliverables and would not need to be particularly made for the structural fire analysis. By starting the workflow from a CAD model, it becomes relatively efficient to integrate the structural fire analysis into the overarching design workflow. As shown in Fig. 4, given a CAD (in this case a Revit) model it is straightforward to export the geometry and build both a GiD model and an FDS model.

The model building process including assigning the sections, materials, and simulation variables can proceed in parallel in collaboration between the fire and structural engineers in FDS and GiD respectively. Before the fire analysis is performed in FDS, thermocouples must be assigned within GiD and exported to FDS. Exporting the thermocouples defined in GiD to FDS is directly performable from the GiD menu in Fig. 4. The format of the exported thermocouple file has been set to be that of the FDS file format so that it can simply be copied directly into the FDS script, with more information about

presented in section 3.3. By automating the creation of the thermocouples, the information transfer becomes a one-way process from the GiD model (structural engineer) into the FDS model (fire engineer). This eliminates the need for manual mapping of thermocouples between the two computational domains (structural and fire) and would reduce the amount of replicated work on both models.

The fire simulation may begin immediately after the thermocouples file is generated and imported into the FDS model. FDS then generates a series of numbered gas temperature files that are to be used in the HT analysis. To perform HT analysis, the information of each section at which a thermocouple was assigned must be aggregated into a unified data file. This data file is generated in the working directory of the GiD model directly from within the GiD interface and will collect the section information automatically from every element that is assigned a thermocouple without the need for any additional user input. Once the FDS fire simulation is completed, the gas temperatures are translated via the Python translation script, which is discussed in section 3.3, into OpenSees HT-compatible boundary condition files containing gas temperatures [49]. Each of the FDS gas temperature files corresponds to the location of a single thermocouple and will have associated with it a single line in the HT data file. To run the heat transfer analysis the user then manually copies the FDS-generated temperature files into the directory of the GiD model and calls the heat transfer process from the GiD OpenSees interface. Considering that each of the heat transfer analysis constitutes the solution of a full FEM problem for thousands of timesteps, a parallel programme was written to cut down on the total computational time required by distributing the workload over multiple processors. This is particularly useful for larger models containing thousands of thermocouples, and hence requiring thousands of HT

analyses. Details of the HT analysis script used and the parallel programme are discussed in sections 3.4.1 and 3.4.3 respectively.

The HT analyses result files are placed in a sub directory within the GiD project working directory. Depending on section type, each HT analysis output consists of a thermal load file containing either 15 points for beam-column elements, or 9 points for shell elements. HT analyses performed for a composite section generates both a shell and a beam-column element thermal load files. The HT result files are associated with the mesh elements via the assigned thermocouples. Finally, an OpenSees script containing all sections and both ambient and thermal loading is generated and run from within GiD, with the output results then compiled into a GiD database allowing for a level of post processing that was not feasible before in OpenSees for fire.

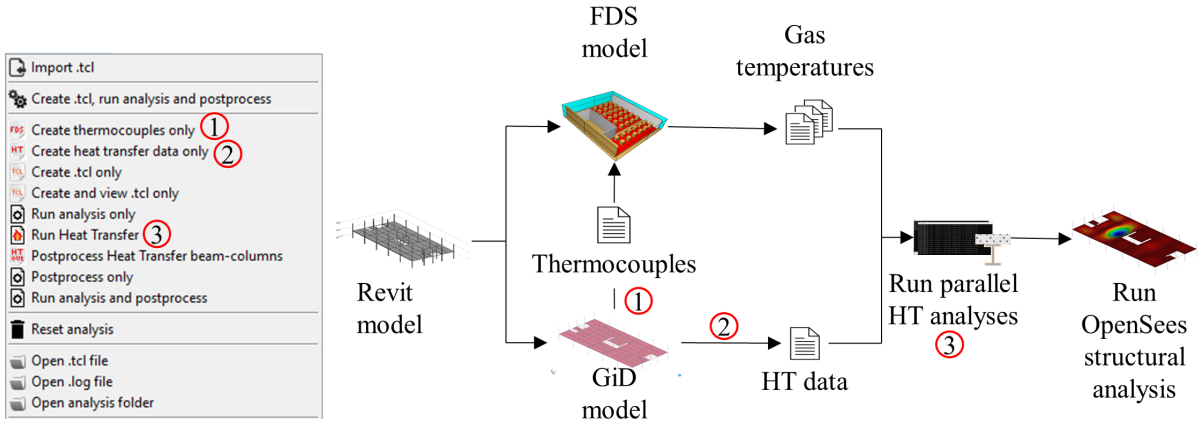


Fig. 4. Workflow for the ISE developed in this research incorporating fire simulation, heat transfer, and structural analysis

### *3.3. FDS and Thermocouples*

FDS can output temperatures, velocities in all dimensions, extinction coefficients, heat fluxes, and more. For HT analysis, the most relevant quantities are heat fluxes and temperatures that are applied as thermal boundary conditions. There are various methods to extract this data from the FDS simulation,

particularly: (1) Device output and (2) Plot3D (BNDF for solid phase devices). In the former, devices, which are the thermocouples created in GiD, are installed at a point location where a quantity needs to be monitored over the course of the fire simulation. The output from the fire simulation provides a time history of the quantity in a comma-delimited file. Only the data required by the user at the thermocouples locations is recorded which reduces computational cost significantly. The thermocouples do not have to conform to the mesh of the FDS model as FDS automatically interpolates the results to their locations. Therefore, the thermocouples in GiD do not affect the GiD mesh and do not enforce any mesh modifications. However, if after the simulation the user requires data at an unrecorded location then the entire simulation must be restarted.

The Plot3D method, on the other hand, records the required gas parameter (temperature, velocity, etc) in binary form for each timestep and for each cell volume of the computational domain. This allows the user to access the results at any location after the simulation but comes at the cost of a higher computational demand and need for larger data storage. This can be a limiting factor for the models of large and complex buildings where the number of cells may be in the millions. The ISE presented in this paper streamlines the creation of FDS thermocouples, and so the first approach is used where only the required FDS data is recorded. The gas temperatures obtained from the FDS simulation are translated via a python script into a time-temperature data format suitable for HT analysis in OpenSees [49].

### *3.4. Automated and fast heat transfer*

#### *3.4.1. Heat transfer script and HT data*

To facilitate heat transfer within the ISE, a selection of predefined 2D heat transfer sections, shown

in Fig. 5, were built into a parametric script that is run by OpenSees. The script receives a series of user-defined parameters defining the type of the section (composite beam, slab, regular I section, or stiffened I section), its dimensions, type of protection material and its thickness if any, and the properties of the fire and its duration. Each of the predefined sections was built up from rectangular 'block entities' which are then joined together using equal degree of freedom constraints between their boundaries as shown in Fig. 6 (a) and (b). This constraint was also used between the blocks representing the concrete 'top flange' of composite beam sections and the top flange of the attached steel beam, as well as between the thermal protection and steel/concrete of the protected sections as shown for a protect I-section in Fig. 6 (b). Temperature boundary conditions are applied around the perimeter of the I-sections, and to the underside of the slab and composite beam sections as the figure shows. The gas temperature boundary condition can be set to the standard fire, hydrocarbon fire, or user-defined fire. The first two thermal exposure types refer to automatically generating the gas temperatures based on the standard fire and the hydrocarbon fire. This is useful for design applications using the ISE particularly at the preliminary design stage where initial sections and fire protection need to be chosen, before detailed FDS analyses are performed if needed. The user-defined exposure is an abstraction for a customised temperature-time exposure that is used for coupling with FDS in the ISE. Ambient boundary conditions are applied at the top surface of the slabs and of the 'top flange' of the composite beam sections. Both convection and radiation are considered at these locations, with an average convective heat transfer coefficient for each of the fire and ambient boundary conditions defined by the user and used to calculate the heat flux from the gas temperatures predicted by FDS.

By utilising gas temperatures instead of adiabatic surface temperatures or heat fluxes it is possible

to refine the HT analysis by calibrating for the value of the average convective coefficient for each member or, more accurately, a local heat transfer coefficient for each location of the structural member. This is done by using time average velocities, temperatures and characteristic length-scales for the structure. The method to do this has been explored in detail by Jowsey [50]. In FDS, in the case of heat fluxes, to obtain them in an accurate manner it is needed to fully couple the CFD and the FE model. This is highly inefficient because the characteristic time scales in the gas phase are much shorter than in the solid phase, thus the need to transfer a heat flux every step of the CFD is a problem. If adiabatic surface temperatures are used, then the heat transfer model needs to be simplified into a single temperature, this requires the definition of constant heat transfer coefficients for the entire cell of the CFD. This can be highly imprecise. Instead, by separating the CFD results and extracting the properties of the cell (like gas temperature), these can be averaged in time in a manner consistent with the characteristic time scale of the solid and the information transferred only at a rate consistent with what is needed. Averaging the gas phase properties over the volume of the cell does not introduce a significant error because the spatial distribution in the gas phase does not vary significantly. Nevertheless, the uncoupled system now allows to carefully assign heat transfer coefficients in a refined manner on the structure. This tackles the most significant source of error.

Mesh size is automatically selected for the section by the script based on section dimensions, ensuring that at least four elements are used throughout the thickness with a maximum element length of 15 mm. Further refinement in mesh size does not significantly affect the results and thus the meshing options are considered adequate. If the user wished to change the minimum element size, then this can be easily done by changing the clearly outlined limit variables in the script under the heading “meshing

parameters".

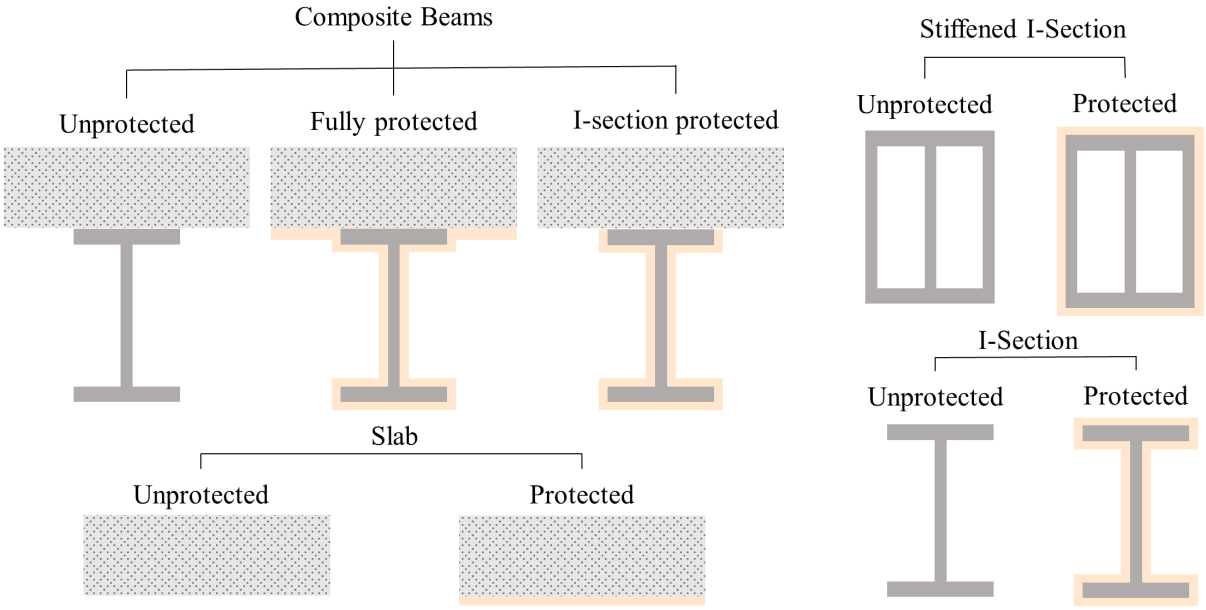


Fig. 5. Section types developed for automatic heat transfer analysis using the parametric HT script developed as a part of this research

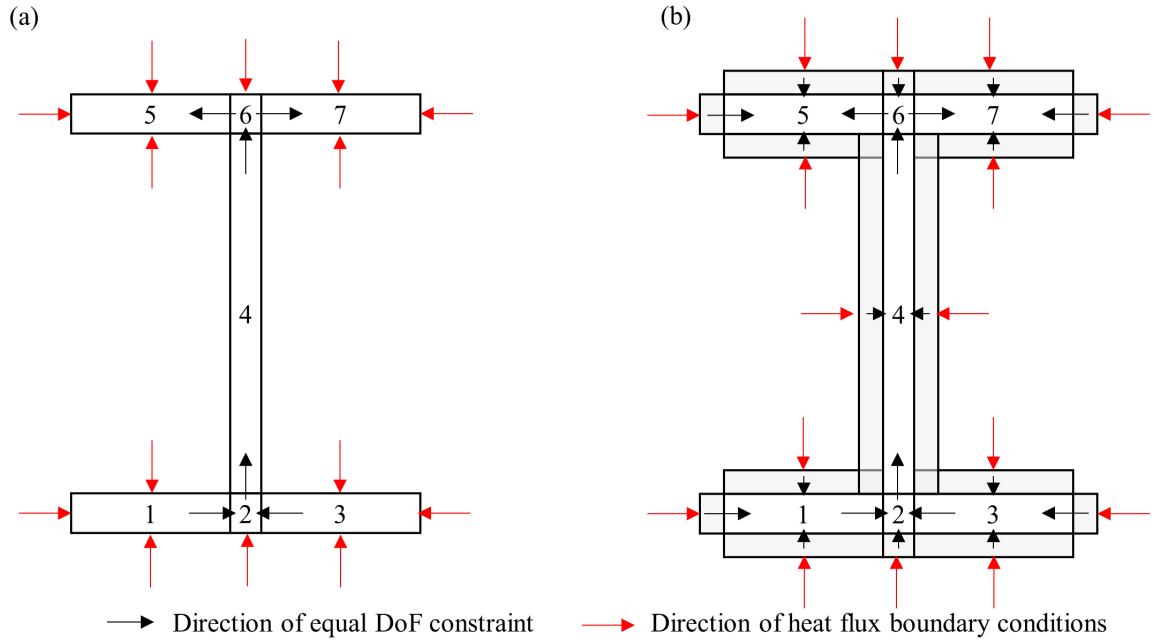


Fig. 6. Constraints applied in the developed HT script to block entities for (a) unprotected I-section, and (b) protected I-section

### *3.4.2. Validation of HT parametric script*

One of the protected composite beams tested by Choe et al. [39] and studied by Li et al. [38] was modelled using the parametric heat transfer script and was run using OpenSees. The beam was a typical W18×35 wide flange beam protected with 19 mm of the Carboline variant from Li et al. [38], and an unprotected light weight concrete slab 83 mm deep. A convective heat transfer coefficient of 25 W/m$^2$K was used with the experimental temperature-time curve for a 100-minutes HT analysis running with a time step of 5 seconds. Unfortunately, there is currently no functional material model for lightweight concrete available in OpenSees, and so the properties of normal weight concrete were used for the concrete 'top flange' of the composite beam. The Eurocode lumped temperature iterative method [41,51], which ignores the small heat capacity of the insulation, was also used to predict the temperature of the steel section to provide a baseline prediction for comparison with the results of the HT analysis model. The same timestep of 5 seconds was used for this analysis. The simulation results from the OpenSees HT analysis as well as the predictions of the numerical simulation performed by Li et al. [38] and the experimental results are compared for the web and top flange of the steel section in Fig. 7 (a) and (b) respectively. For the web, which was heated from both sides and is the thinnest part of the steel section, the results of the numerical simulations and lumped temperature predictions are in very good agreement. Likewise, the numerical predictions by OpenSees and from Li et al. [38] are very close for the top flange. This indicates that the current computationally inexpensive 2D OpenSees script is producing predictions that are of a similar quality to a significantly more sophisticated 3D numerical simulation. However, both the OpenSees and the Li et al. [38] numerical results overestimate the temperatures reached in the steel beam by about 140 °C for the web and about 160 °C for the top flange.

Both the OpenSees and Li et al. [38] numerical results differ from the experimental observations in the top flange because of the complexity of the actual radiative heat flux and hot gas movement at the interface between the steel beam and the slab. Such complex phenomena may require a significantly more sophisticated three-dimensional approach including detailed models for turbulence and radiation to capture accurately. This error may also be due to inaccuracies introduced by the thermal material model which was adapted from Li et al. [38] and implemented into OpenSees in this work. However, as the OpenSees results overestimate the steel temperatures, it is believed that the presented level of accuracy is sufficient for the thermomechanical analyses performed as part of the ISE.

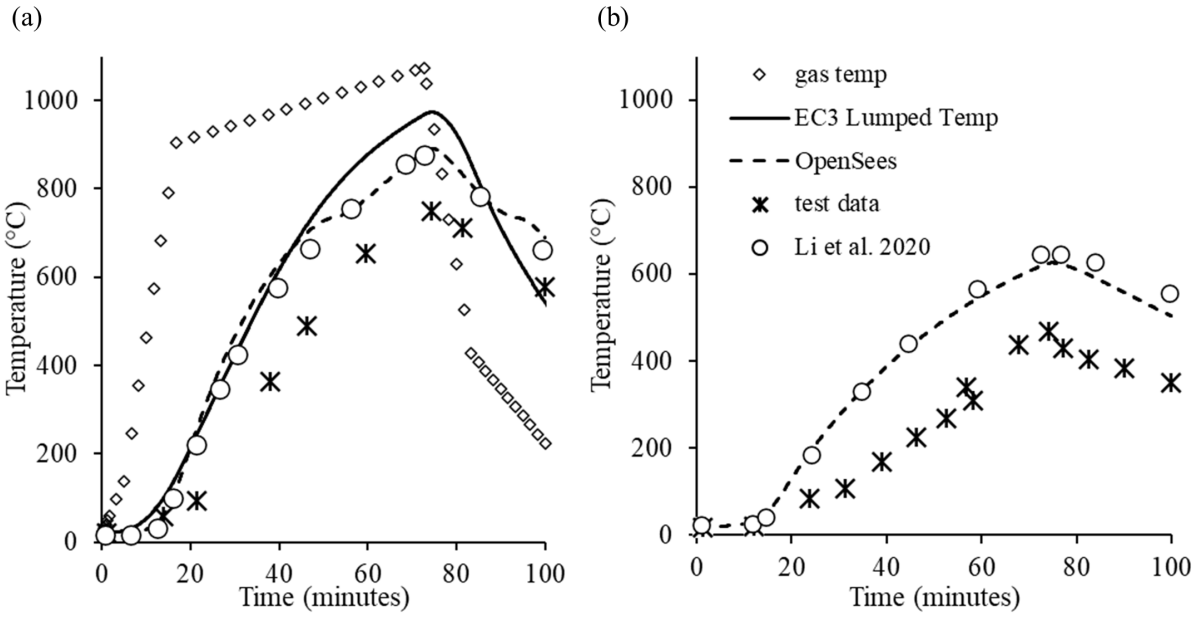


Fig. 7. Heat transfer results from OpenSees using the developed HT script compared with predictions using the EC3 lumped temperature and presented against experimental and numerical results from [38] for (a) web and (b) top flange

### *3.4.3. Parallel heat transfer analyses*

Substituting a series of 2D HT analyses for 3D HT analyses to map gas phase temperatures from FDS to solid phase temperatures in the structural elements reduces the computational load considerably

while maintaining a good level of accuracy [36]. In large or complex models, the number of required thermocouples and corresponding HT analyses can number in the thousands which then once again increases the computational cost. As the intermediary step between fire simulation and thermomechanical simulation, HT analysis should be performed more efficiently but without sacrificing accuracy. The HT script presented earlier sought to optimise the HT mesh and make sure that each HT problem solved is relatively inexpensive. Since each individual problem is inexpensive, it is possible to perform multiples of these problems simultaneously on the same machine. Modern processors including those in portable devices such as phones and tablets are now routinely equipped with multiple computing cores that enable efficient multiprocessing. This fact can be exploited by assigning each processor a unique HT problem to solve thus performing multiple HT analyses at the same time and reducing the overall analysis time.

To do this, a programme based on the manager-worker paradigm for multiprocessing was written in C++ with the MS-MPI library. This programme is included as part of the GiD OpenSees interface and is assigned to perform HT over four processors by default. The programme handles multi-processing by passing messages containing instruction sets between processors. Fig. 8 (a) through (d) explain how the programme works:

(a) When HT is called from within the GiD OpenSees interface, a processor designated with an ID of 0 is set as the ‘manager’, and is given the GiD-generated HT data file. The manager parses this file and separates it into a list of individual commands each of which constitutes the data for a single HT analysis.

(b) The manager sends a single command to each processor dedicated to the HT task except itself.

Each of these processors, which are known as the 'workers', starts an instance of OpenSees and executes the HT problem that was assigned to it.

(c) When any of the processors completes the HT analysis it was assigned it notifies the manager that is now free and available to perform another task. The manager in response assigns that worker another HT problem to solve. The results of the completed analysis are saved within the GiD project directory, and a log file is also generated containing information about the success or failure of the analysis.

(d) Upon completion of all HT tasks, the manager 'retires' the workers and then proceeds to inspect all generated log files. Based on the information in the log files, the manager writes a report file containing the identification number of each HT transfer problem and whether this problem was analysed successfully or not. If the problem failed to be analysed the manager indicates in the report file whether this failure occurred due to divergence of the numerical solution procedure or because of other issues such as incorrect data passed to the HT script.

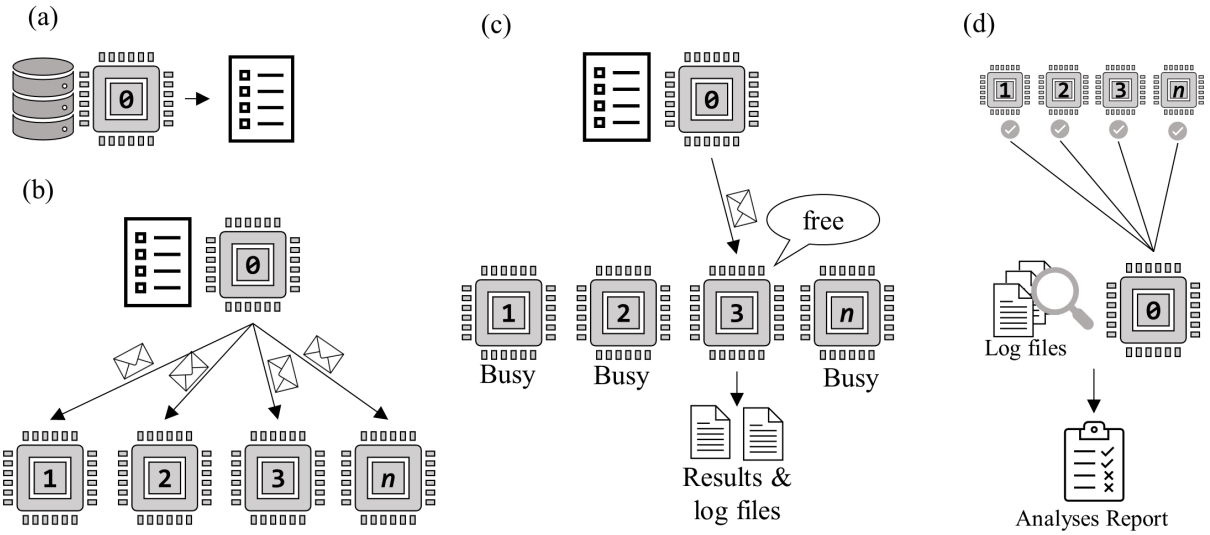


Fig. 8. The manager-worker paradigm developed as part of this research for heat transfer (a) manager breaks problem database into individual command lines, (b) manager distributes work to

workers, (c) once a worker completes a task and produces an output it asks for a new job from the manager, and (d) once all jobs are done workers are retired and manager checks log files and generates status report for the analyses

## 4. Application to large scale structural fire modelling

### *4.1. The Cardington Large Compartment Test*

The Cardington large compartment test was the largest test performed during the Cardington series of tests, and it involved over 340 $m^2$ of the floor area of a single floor. This experiment was chosen as a demonstration case for the current work. This is because (a) it represents a realistic form of construction used for tall and composite buildings, and (b) it is a large-scale test thus posing significant practical constraints to the classical simulation workflow. The goal of this demonstration is to showcase the efficiency of the presented simulation environment in handling large models, not to investigate the real behaviour of the Cardington large compartment test as that has been done by researchers in the past [52,53]. The first step towards this goal is to create a 3D Revit or other CAD model, such as the one presented in Fig. 9 (a), which has the dimensions and gridlines shown in Fig. 9 (b). A fire based on the general conditions of the experiment is then generated using FDS, accompanied by generation of a GiD model. HT based on the FDS results is then performed, and the structure is analysed and results are finally discussed.

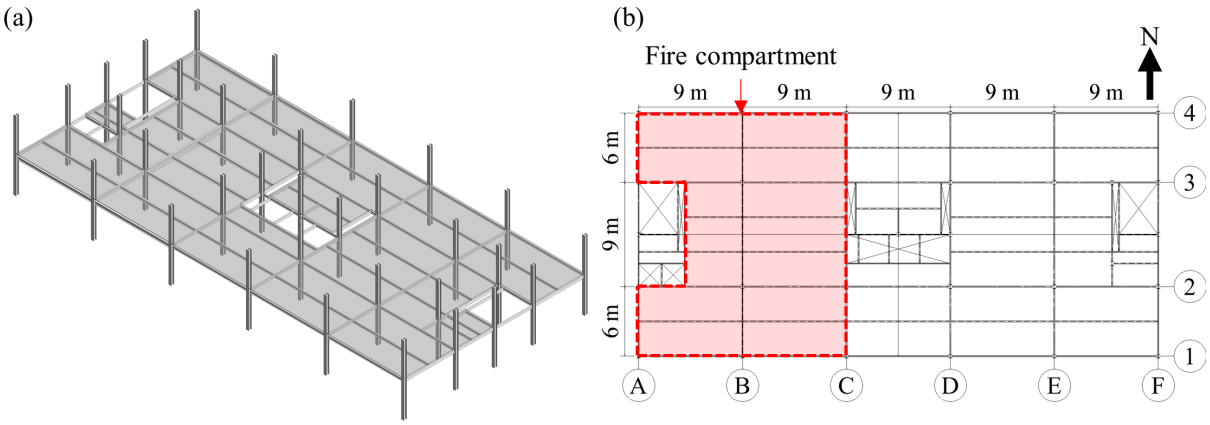


Fig. 9. Revit model for the Cardington building built for the demonstration of the ISE (a) 3D view, and (b) plan view

### *4.2. FDS Simulation*

As per the integrated simulation workflow, an FDS model of the compartment used in the Cardington large enclosure test was created using geometrical information exported from the Revit model. Both north and south faces were assumed to be completely open and would allow for unhindered air flow. Fig. 10 (a) shows the compartment geometry and Fig. 10 (b) the computational domain. Wood cribs were used to fuel the fire of the test, and despite their practicality and widespread use for experiments, modelling their combustion remains an involved task. It has been shown that due to the complex chemical kinetics involved and scale of individual timber pieces used high-fidelity simulation of burning cribs may require a mesh size in the order of at most 0.05 m [42]. In this study, the cribs were simplified and abstracted as a collection of three 1 m × 1 m × 0.4 m blocks in FDS allowing for utilisation of a coarser mesh resolution that detailed simulation of the cribs would prohibit. To allow for the effect of porosity which would increase the burning rate due to the free movement of air [54] a 0.2 m gap was set between the blocks of each crib set as shown in Fig. 10 (a). The properties of wood were taken from the SFPE handbook and data available in the literature [54,55]. Mesh sizes of 0.3 m, 0.2 m,

and 0.15 m were tested. The variation of gas temperatures between the three meshes indicated that a cell size of 0.2 m was suitable for the FDS analysis. The blocks were spaced at 1.5 m intervals and simulated a fuel load of 48 kg/m$^2$ (calculated as fuel per floor area), which is more than the fuel load of 40 kg/m$^2$ used in the actual test. As mentioned earlier, this FDS simulation was not intended to explicitly simulate the real test fire using this model but produce realistic spatially and temporally varying gas temperatures to demonstrate the ability of this framework to utilise complex, CFD-based heating fields for thermo-mechanical analysis of complex structures. An ignition temperature of 320 °C was assigned to the fuel, all of which was ignited using burners set for two minutes at the beginning of the analysis. The *burn-away* method was used to represent decay phase where once the mass of fuel in a cell volume is burnt out, the entire fuel volume would be deleted from the computational domain [42].

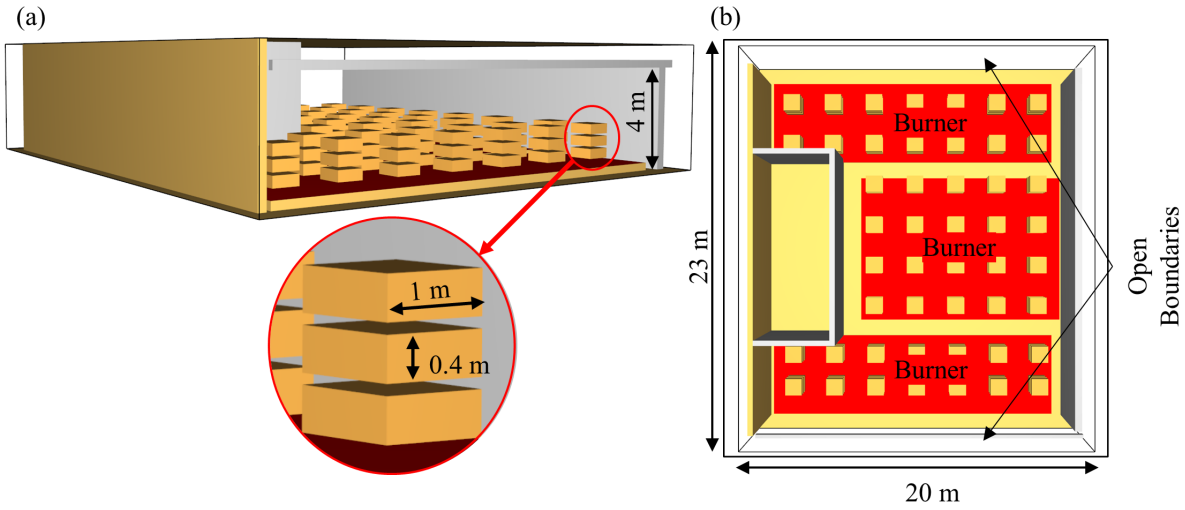


Fig. 10. Fire compartment and computational domain of the FDS model built to produce a CFD-based heating fields for the demonstration of the ISE (a) fire compartment and fuel abstraction, and (b) computational domain dimensions

Fig. 11 shows the fire simulation at three different time intervals. After the initial ignition event,

which lasted for two minutes, the burner was turned off and all the fuel in the compartment had ignited as seen five minutes into the simulation in Fig. 11 (a). 45 minutes into the simulation, some of the fuel blocks already burnt out and were removed from the computational domain as per the burn-away method, as seen in Fig. 11 (b). Fig. 11 (c) shows the state of the simulation after two hours when all the fuel in the compartment was burnt out and only smoke remained within the compartment. The gas temperature contours for 3 m above the compartment floor for time stamps of 15 minutes, 60 minutes, and 120 minutes are plotted in Fig. 12. The highest temperatures are reached within the middle of the fire compartment, while the temperatures near the openings are significantly lower. This variation can be explained by the volume of cool air entering the fire compartment from the openings and mixing with the hot gases thus reducing the overall gas temperatures in the regions closest to the ventilation.

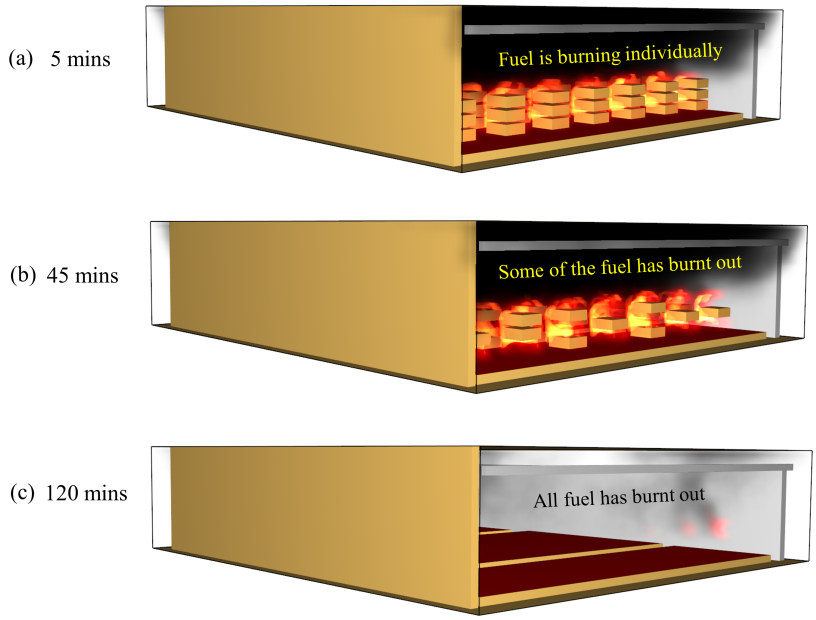


Fig. 11. The demonstration FDS simulation showing (a) all fuel in the compartment is burning (b) some of the fuel is burned out (c) fuel fully consumed

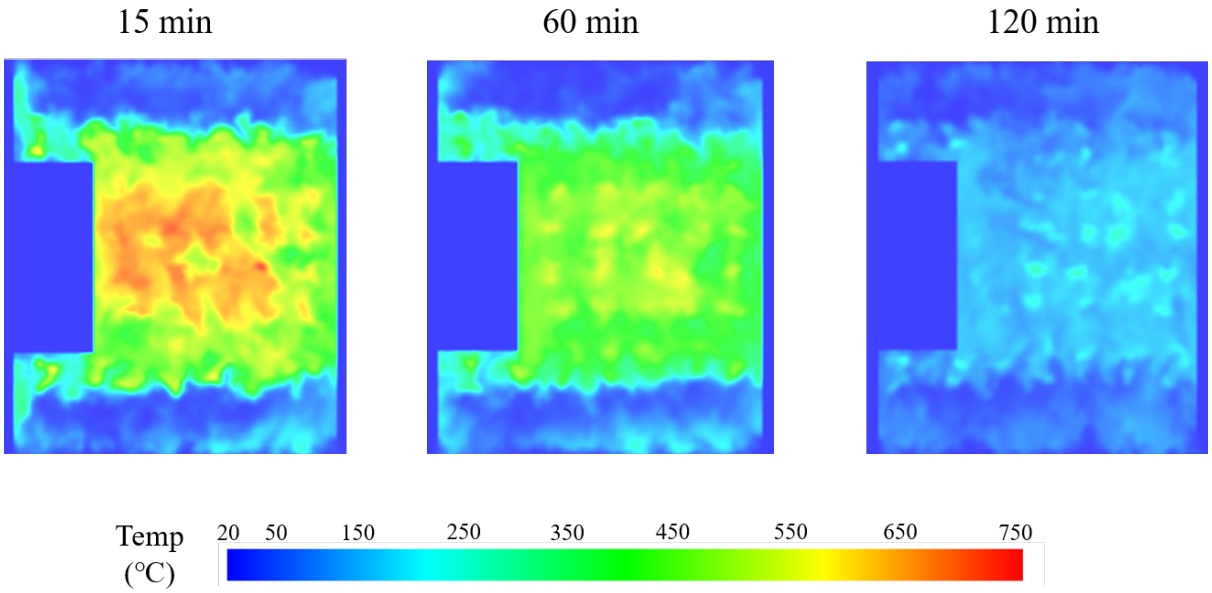


Fig. 12. Temperature contours at a height of 3 m from the floor extracted from the presented FDS model

### *4.3. Materials, thermocouples, connectivity, and meshing*

The floor of the Cardington building consisted of a 130 mm thick ribbed slab with 6 mm diameter 200 mm × 200 mm wire mesh. The ribs were 55 mm deep, and the steel decking had a thickness of 0.9 mm. Full connectivity between the slab and the floor framing was ensured using shear studs with a diameter of 19 mm. To represent the orthotropic effect of the ribs, researchers have used purpose-built finite elements [56,57], combination of beam and shell elements to represent the ribs and continuous portions respectively [29], and simplifications where the ribbed portion of the floor is ignored [8]. While the first approach may be the most sophisticated, its outcome is highly dependent on the quality of implementation employed, and its non-standard formulation means that it may not be widely available. OpenSees for fire does not yet have a working and validated ribbed section representation, although this is currently being developed. The second approach using beam elements to represent the ribs is feasible in OpenSees and has been used for structural fire simulation before [29]. The main issue with

this approach is that it introduces a very large number of constraint conditions to link the nodes of the ribs and continuous segments of the slab together. While this may be tolerable in smaller models, the added computational expense may easily outweigh the benefit of potential added accuracy in larger models. Finally, by ignoring the effect of the ribs altogether one may get a far less expensive model that could possess a satisfactory level of accuracy depending on the purpose of the model. The intention of the presented simulation environment is to make more representative analyses feasible, and so ignoring the effect of the ribs is undesirable. To overcome these difficulties, a different approach is employed for the demonstration case where groups of ribs are aggregated together and then represented using shell elements.

Two layered shell sections were defined for this purpose, a 130 mm section to represent the ribs, and a thinner 70 mm representing the continuous portion of the slab. These sections were alternatingly applied to the floor slab in the fire region as shown in Fig. 13. As will be shown later, representation of the thicker and thinner parts of the slab helps capture, although in a simplified fashion, the complex thermal state and thus thermomechanical response that is experienced by ribbed floor slabs.

The reinforcement in the slab was represented using the rebar-mesh approach detailed in [29], and was assigned a yield strength of 460 MPa, and hardening parameter of 0.015. The concrete was modelled using the thermomechanical CDP implementation and was modelled with a compressive strength of 35 MPa, tensile strength of 4 MPa, modulus of elasticity of 26 GPa, and compressive and tensile strain multipliers $m$ and $n$ of 10. This assumes that the concrete would lose all strength at 10 times its compressive and tensile plastic strain values. Consideration of plasticity in the beam-column elements was done by using fibre-based sections which allow for consideration of plasticity throughout

the section and across the integration points over the element. The fibre edge sizes were between 10 and 40 mm depending on the section size, which results in a minimum of 30 fibres used to represent each beam section. Perfectly stiff connections between the beams, and between the beams and columns were assumed. The assumption of stiff connections has been shown to be reasonable in previous work on composite floors in fire [11,29,58,59]. The modelling more realistic connections is an important avenue for the development of the ISE in the future. The large compartment test took place on the third floor, and so the load from the five floors above it was applied to its column tops, which were allowed to translate vertically but restrained in all other degrees of freedom. A static analysis of the test floor with a uniform dead load of 5.4 kN/m2 was performed, and then the reactions at the columns were extracted, multiplied by number of floors above, and applied to the top of the columns for the thermomechanical analysis. The column bases were assumed to be fixed.

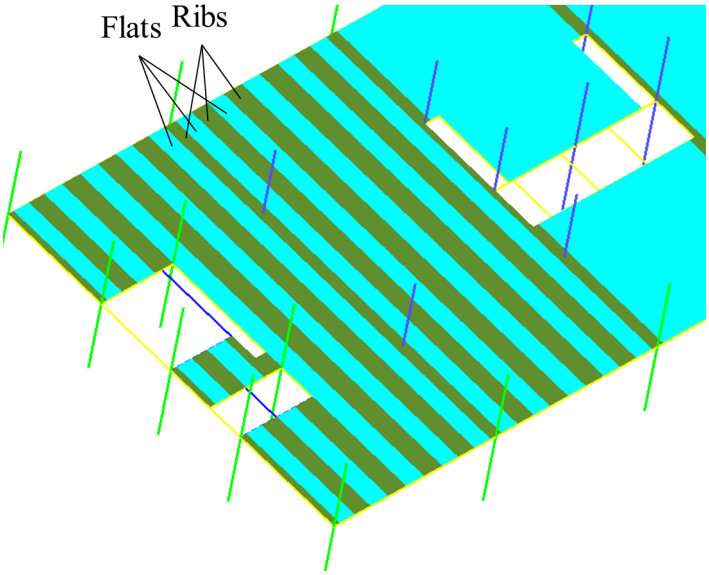


Fig. 13. Distribution of rib and flat sections for the slab in the GiD model of the demonstration example

The distribution of the thermocouples within the floor is governed by the number of geometric

divisions the user enforces over the model. For the demonstration case, slab thermocouples were distributed at intervals of *approximately* 1 m as shown in Fig. 14 (a). Likewise, the thermocouples for composite beams were spaced approximately 1 m apart, with the assumption that their temperatures and HT results apply over a 0.6 m wide 'top flange' area. Each surface shown in Fig. 14 (a) has a thermocouple located in its centre. The thermocouples corresponding to composite beams supersede slab thermocouples if both types of thermocouples were applied to the same surface. As shown in the *section 2.3.*, the connectivity between the steel beams and their concrete 'top flanges' was established automatically at the nodal level by applying 'composite section beam' and 'composite section slab' conditions over their respective geometric lines. The floor slab shell elements were offset by 70 mm from the beam elements, and 'beam' rigid links that transfer both rotations and translations were chosen here to represent the full composite action and incorporate the dowel action caused by differential heating. The mesh used was relatively fine with element length set to 0.3 m, resulting in at least nine elements representing each slab thermocouple, and six elements representing each composite beam 'top flange' at each thermocouple location as shown in Fig. 14 (b). The fine mesh used here was chosen to allow the distribution of concrete damage to spread in a more natural manner reducing the mesh-dependency reported for distributed cracking methods [60]. As per the workflow of the ISE, at each thermocouple location an appropriate HT analysis was performed, and the results were then automatically applied to the correct mesh elements. In total, there were 996 thermocouples and over 11,000 nodes, 7,200 shell elements, and 3,600 beam-column elements. Performing the thermomechanical analysis in OpenSees solver took just under 4 hours on a regular i7 3.00 GHz desktop computer.

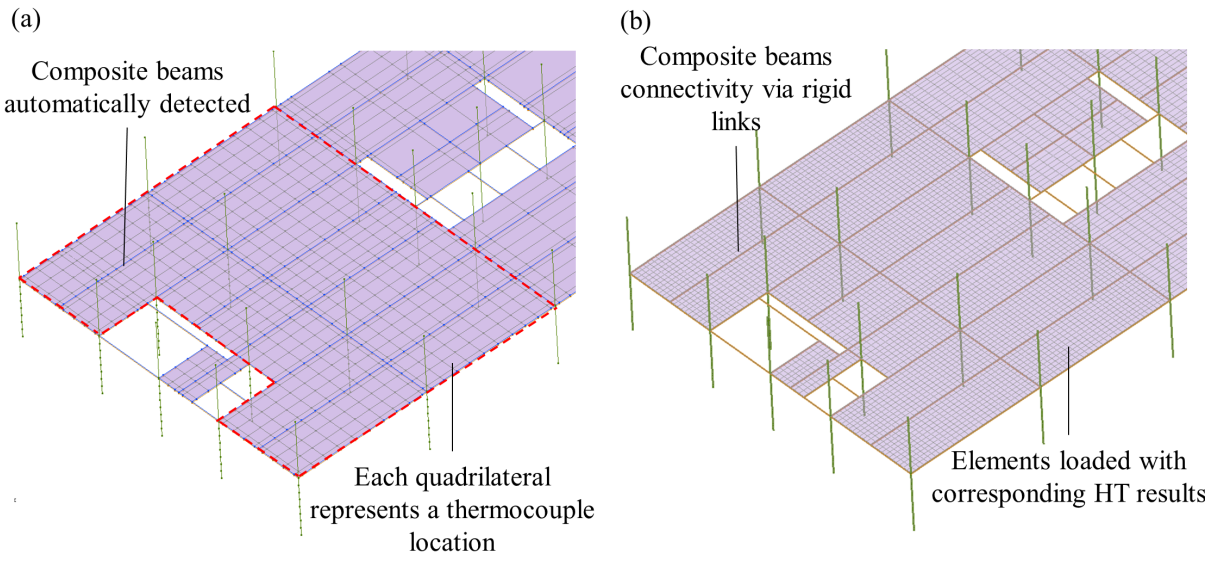


Fig. 14. The presented GiD model (a) geometry and thermocouples distribution, and (b) mesh

### *4.4. Heat transfer results*

Representing the ribbed slab using two types of shell element sections allowed the effects of spatial variation of temperature and the heat-sink effect of composite beam 'top flanges' to be clear after the HT analysis. Fig. 15 (a) presents the evolution of temperature in the bottom layer of the layered slab sections over 90 minutes of the fire. As discussed in *section 4.2*., the hottest gas temperatures were located within the middle of the fire compartment within the region enclosed by gridlines B, C, 2, and 3 (Fig. 9 (b)). The perimeter of the building outside gridlines 2 and 3 stayed relatively cool throughout the analysis. The hottest temperatures within the floor slab were achieved after about 1 hour of heating, with the thinner portions of the slab reaching higher temperatures faster due to their lower thermal mass. Moreover, the presence of composite sections resulted in the initial emergence of cooler zones along the length of the beams, such as that seen 15 minutes into the fire over the largest floor beam along gridline B and within gridlines 2 and 3. This phenomenon is reversed during cooling, which takes place after 60 minutes. At 75 minutes it is observed from Fig. 15 (a) that the shell elements atop the composite beams remain hotter than the adjacent slab. The composite steel beams below these segments initially

acted as thermal barriers and heat sinks protecting the slab from direct convection and radiation during heating. During cooling, the energy that the steel beams absorbed was slowly released into the atmosphere while preventing the slab from cooling rapidly. This effect can still be seen even 90 minutes into the fire and 30 minutes after the highest temperatures were reached. The top surface of the slab experiences a different thermal history. As shown in Fig. 15 (b), the thick and thin layered sections produce a clear effect with the thin sections reaching maximum temperatures of about twice the thicker sections. As expected, the top surface temperatures continued to increase for over 30 minutes after the peak gas temperature was reached.

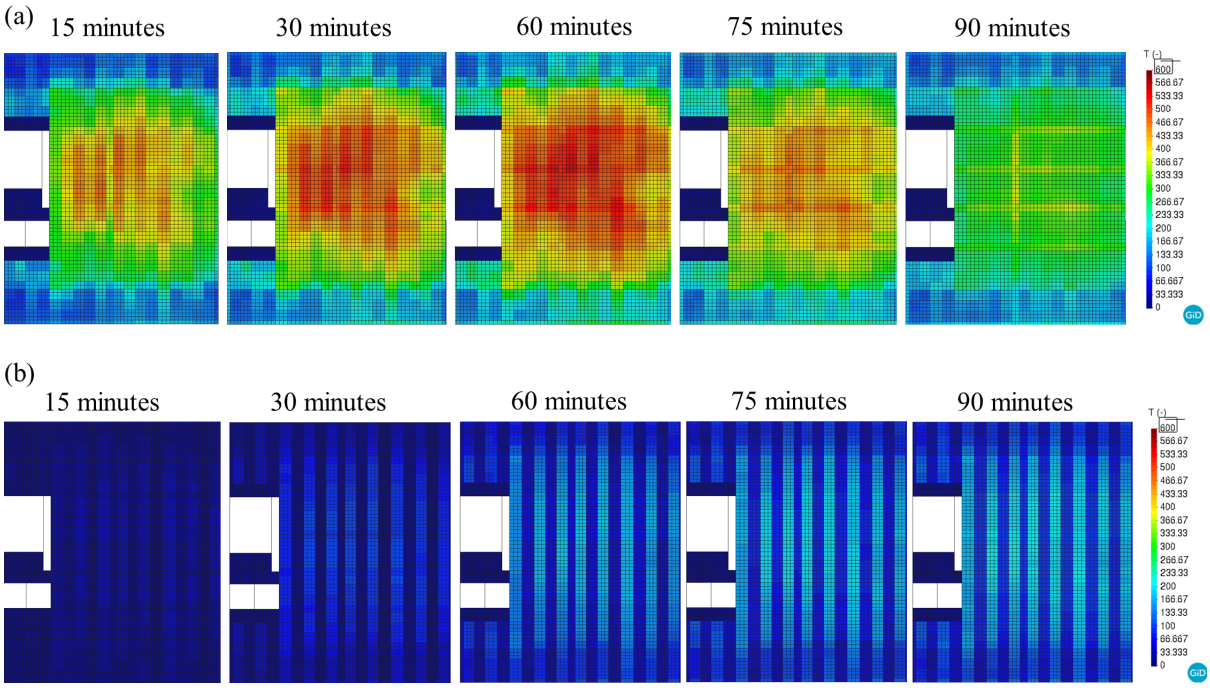


Fig. 15. Temperature growth results after heat transfer in the ISE (a) in the bottom layer of the slab, and (b) in the top layer of the slab

It is noted in Moss and Clifton [52] that the temperature within the fire compartment was generally uniform and could be averaged as shown in the average temperature curve in Fig. 16 (a), which is contrary to the FDS results used in this demonstration which showed spatial variation.

Observation of the experimental data showed indeed that the temperature varies spatially. Fig. 16 (a) also showcases the test data from the test thermocouple 415 located 300 mm from the top of the compartment at the centre of the east bay. Two abnormalities presented in the FDS gas temperature-time curve: an initial momentary spike in temperature reaching 800 °C, and a 'stepwise decrease in temperature after uniform 600 °C temperatures for 60 minutes. The first occurred, as explained in *section 4.2.*, due to the artificial ignition of all cribs at the same time using burners for the first 2 minutes of the analysis. The second phenomenon is an artifact of the prescribed combustion behaviour of the wooden cribs and their abstraction as simple blocks. Because of these reasons, the gas temperatures from the current FDS analysis appear less 'natural' than the average experimental temperature-time curve. However, the overall behaviour and the rate of temperature decay are qualitatively similar to the recorded temperature from the test in the same location. The difference in magnitude between the FDS and experimental results is likely related to the combustion properties of the wood as well as the limitations of the modelling methods used in the presented FDS simulation. This includes the chosen extinction model and the FDS heat transfer coefficients in the cooling phase [45,61]. However, these spatially varied temperatures present by far the more interesting case for both the kind of academic study presented here and for practical application where the conditions for uniform temperatures across a large compartment are unlikely to be met.

Fig. 16 (b) shows the thermal gradient achieved by a composite beam located within the middle of the fire compartment. Since none of the beams in the test were protected, the steel temperature in the bottom flange rises to the proximity of the gas temperature within minutes from ignition. The top flange, however, remains relatively cooler due to the heatsink effect of the slab. The bottom of the slab is tied

to the top of the beam with an equal degree of freedom constraint during the HT analysis and thus is at the same temperature as the top flange. The temperature within the middle of the slab and at the top surface is also plotted demonstrating the nonlinear temperature profile within the concrete 'top flange' of the composite beam. While the temperature in the steel beam and bottom of the slab enters the cooling phase shortly after the peak gas temperatures are traversed, the concrete within the slab continues to heat up to around 90 minutes. It is crucial to note here that the consideration of the steel beam and concrete slab as a unified HT cross-section and as linked structural components enables the development of large thermal gradients and for the effects of these gradients to be considered. It has been shown elsewhere [62] that a thermal gradient on its own is sufficient to trigger tensile-membrane action in thin slabs, and has been recognised as one of the key actions producing large deflections and inducing secondary forces in composite beams [63,64]. The thermal gradient within composite floor beams of large structures should always be considered, as is done in this demonstration and facilitated by the presented ISE.

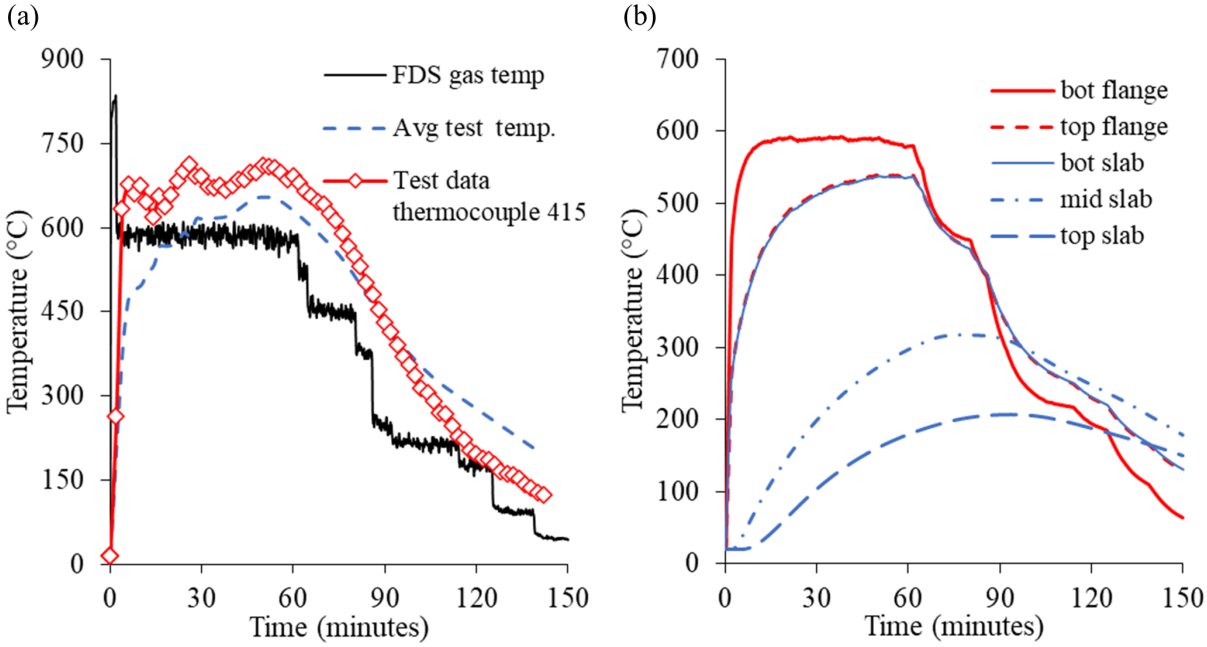


Fig. 16. Temperatures in the model (a) FDS gas temperatures from this work in middle of the compartment compared to the average experimental compartment temperature as presented in [52] and test data for thermocouple 415 from the same location, and (b) thermal gradient achieved in a composite beam subject to the presented FDS gas temperatures

### *4.5. Deflected shape and displacements*

Upon studying the deflected shape in Fig. 17 it is evident that the unheated structure experiences only minor deformations, as expected. The largest deflections occurred in the middle of the fire compartment marked as 'Location 1' in Fig. 17. 'Location 2' was also instrumented, and results were available [52]. The deflection at these two locations is plotted in Fig. 18 (a) and (b) respectively. In addition to the test data and numerical predictions from the demonstration case, numerical predictions from Moss and Clifton [52] are also shown. For completeness, the test temperature-time curve was applied to the model using the integrated environment, and results from that analysis are also shown. The results from the demonstration case are vastly different from the experimental results. This

difference is caused by the different heating regimens the test and demonstration case were subjected to, which becomes evident when the test temperatures were applied uniformly to the heated region. The deflection results very close to the test results at location 1. The application of uniform temperatures across the entire area also meant that location 2 was subjected to the highest temperatures just like location 1, which if the FDS results are taken as a general indicator of 'hot' and 'cool' zones was not the case. These high temperatures caused the composite beams in that region to exceed the experimental results significantly. The very cool temperatures generated by FDS at location 2 resulted in very small deflections at that location as predicted by the demonstration case.

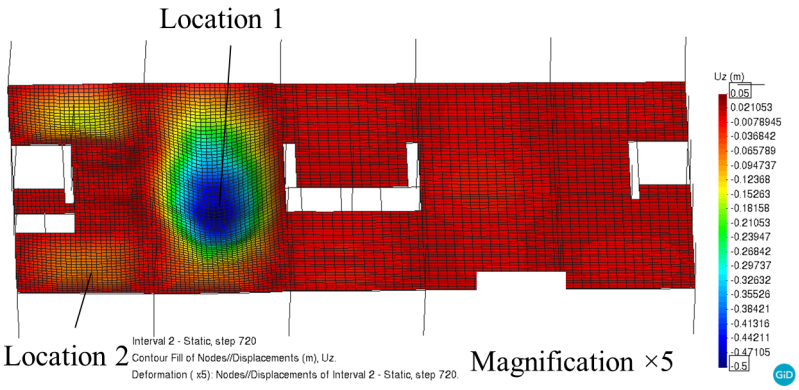


Fig. 17. Deflected shape of the present ISE model subject to FDS temperatures (×5 magnification factor)

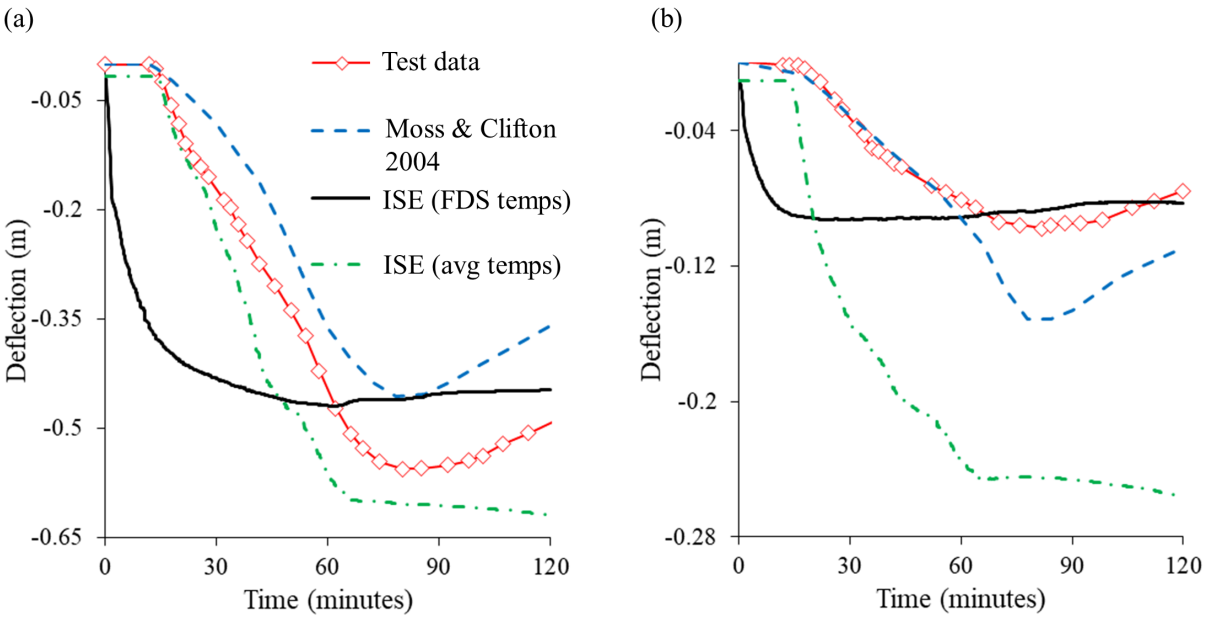


Fig. 18. Deflections data from the experiment and the numerical analysis by [52] compared to the results from the demonstration OpenSees/GiD/ISE model for (a) location 1, and (b) location 2

### *4.6. Damage*

The concrete damage plasticity material model used for the shell elements in this simulation environment is governed by damage parameters that track the accumulation of compressive and tensile cracking and their recovery upon load reversal [29]. Therefore, by tracking the tensile damage variable at the top layer of the concrete, Fig. 19 can present a visualisation of the potential top layer cracking the structure may exhibit. Amongst the clearest indicators of damage observed in composite floors in fire is the early cracking of their perimeters at the locations of connection to large girders and columns [65–67]. This phenomenon seems to present as early as 1 minute into the thermomechanical analysis where the highest damage is first accumulated over the largest composite beam. From there, the damage begins to spread rapidly and from over the composite beams. By the end of the analysis, the top concrete layer is shown to have experienced significant cracking throughout the fire compartment, with damage spreading over to the unheated structure. This is the reason why the lack of high deflections in the

compartments unexposed to fire should not be the only consideration for whether to include them in the analysis. These adjacent bays may play an important role in applying finite restraint to the structure and may experience interesting phenomenon such as extended cracking as shown here and even more clearly in the large-scale experiment presented in Yang et al. [68]. Nevertheless, caution must be advised when interpreting the damage parameter results as they can only give a general idea of the expected damage pattern at a particular layer. Tracking the coalescence, and propagation of through depth cracks, and even discrete surface cracks, requires more sophisticated approaches that employ the extended finite element method [60] or other advanced implementations and solvers.

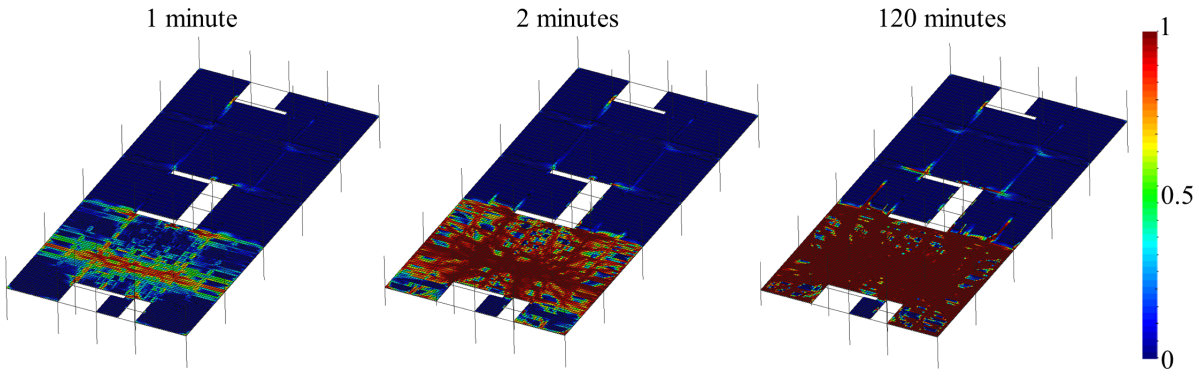


Fig. 19. Postprocessing of the top layer tensile damage output within the developed ISE

## 5. Conclusions

This article discussed recent developments in the simulation of composite and complex buildings in fire, presented an open-source integrated simulation environment that allows for modelling them efficiently, and then used a demonstration study to showcase the abilities of the developed environment. The simulation environment links models built in CAD, fire simulation in FDS, as well as HT and thermomechanical analyses in OpenSees via the GiD OpenSees interface. The GiD OpenSees interface

generates the FDS thermocouples, and the data required for HT, performs HT transfer analysis over multiple processors, assigns the results to the mesh as a thermal load, and produces an OpenSees script for thermomechanical analysis. Finally, GiD combines the results into a database for post processing allowing OpenSees for fire results to be visualised in a way that was not possible before. The key conclusions from this work are:

(1) The OpenSees HT script presented in this paper is capable of accurately assessing the temperatures within protected structural members as shown by validating against experimental and numerical results.

(2) The GiD OpenSees framework was extended to incorporate thermomechanical materials, sections, elements, and loads. In addition, 'thermocouples' were implemented in GiD OpenSees to seamlessly create FDS devices and then use the results for heat transfer analysis in OpenSees. Composite section definition was also added to GiD OpenSees to automatically establish connectivity between the shell elements and beam-column elements representing the concrete 'top flange' and steel section of composite beams, respectively.

(3) The Cardington large compartment test was used a demonstration case for the integrated simulation workflow. A Revit model was built, and its geometric information imported into GiD and FDS. An FDS analysis was run and generated gas temperatures that were significantly higher in the middle of the fire compartment than near the openings. These temperatures were monitored over 996 thermocouple locations and used for heat transfer analysis and then thermomechanical analysis. The maximum deflections achieved were within about 20% of the experimental deflections but followed a different pattern. This was primarily caused by the

difference between the FDS simulation and the real fire. Damage patterns tracked using the concrete damage parameters point towards cracking initiating from above the largest floor beam and extending over the composite beams due to the restraint. Damage enveloped the entire compartment by the end of the test and even extended into the unheated portions of the floor.

(4) Performing a simulation of the scale and level of details as the demonstration example would be a hugely cumbersome task if not for the ISE handling the mapping of thermocouples, generation of HT data, and performing of HT and then assigning the results and connectivity to the mesh. Within this environment it is now possible for researchers and engineers to tackle large problems more effectively and efficiently while making better use of the computational power that is now routinely available at their disposal.

(5) All the developments mentioned in this work are open-source, and interested readers are encouraged to test these tools for themselves. The required software is available for download on GitHub [27,28,49].

**Acknowledgements**

This research is funded by the RGC Hong Kong GRF Scheme (No. 15220618) and SLDRCE Open Fund (SLDRCE20-02) from the State Key Laboratory of Disaster Reduction in Civil Engineering.

## References

[1] J.L. Torero, Grenfell Tower: Phase 1 Report GFT-1710-0C-001-DR-01, London, UK, 2018. https://www.grenfelltowerinquiry.org.uk/evidence/professor-jose-l-toreros-expert-report-supplemental.

[2] L. Bisby, Grenfell Tower Inquiry Phase 1 Final Expert Report, Edinburgh, UK, 2018. https://www.grenfelltowerinquiry.org.uk/evidence/professor-luke-bisbys-expert-report-supplemental.

[3] A.A. Khan, S. Lin, X. Huang, A. Usmani, Facade Fire Hazards of Bench-Scale Aluminum Composite Panel with Flame-Retardant Core, Fire Technol. (2021). https://doi.org/10.1007/s10694-020-01089-4.

[4] A.A. Khan, A. Usmani, J.L. Torero, Evolution of fire models for estimating structural fire-resistance, Fire Saf. J. 124 (2021). https://doi.org/10.1016/j.firesaf.2021.103367.

[5] BSi, EN 1991-1-1:2005 Eurocode 1: Actions on structures, (2005).

[6] A.A. Khan, R.V.V. Domada, X. Huang, M.A. Khan, A. Usmani, Modeling the collapse of the Plasco Building. Part I: Reconstruction of fire, Build. Simul. (2021) 1–14. https://doi.org/10.1007/s12273-021-0825-4.

[7] NIST, NIST NCSTAR 1A: Final Report on the Collapse of the World Trade Center Building 7, 2008. http://www.nist.gov/customcf/get_pdf.cfm?pub_id=861610.

[8] T. Gernay, N.E. Khorasani, Recommendations for performance-based fire design of composite steel buildings using computational analysis, J. Constr. Steel Res. 166 (2020) 105906. https://doi.org/10.1016/j.jcsr.2019.105906.

[9] K. McGrattan, S. Hostikka, R. McDermott, J. Floyd, C. Weinschenk, K. Overholt, Sixth edition fire dynamics simulator technical reference guide volume 1 : mathematical model, NIST Spec. Publ. 1018. 1 (2015). https://doi.org/10.6028/NIST.SP.1018-1.

[10] F. McKenna, G. Fenves, M. Scott, OpenSees: Open System for Earthquake Engineering Simulation, (2000). https://opensees.berkeley.edu/.

[11] J. Jiang, A. Usmani, G.Q. Li, Modelling of steel-concrete composite structures in fire using OpenSees,

Adv. Struct. Eng. 17 (2014) 249–264. https://doi.org/10.1260/1369-4332.17.2.249.

[12] J. Jiang, L. Jiang, P. Kotsovinos, J. Zhang, A. Usmani, F. McKenna, G.-Q. Li, *OpenSees* Software Architecture for the Analysis of Structures in Fire, J. Comput. Civ. Eng. 29 (2015) 04014030. https://doi.org/10.1061/(ASCE)CP.1943-5487.0000305.

[13] J. Jiang, P. Khazaeinejad, A. Usmani, Nonlinear analysis of shell structures in fire using OpenSees, (2012).

[14] M.A. Orabi, A.A. Khan, A. Usmani, An Overview of OpenSEES for Fire, Proc. 1st Eurasian Conf. OpenSEES OpenSEES Days Eurasia. (2019) 1–6.

[15] Y. Jiang, Development and application of a thermal analysis framework in OpenSees for structures in fire, The University of Edinburgh, 2012.

[16] T. Kartalis-Kaounis, V.K. Papanikolaou, GiD + OpenSees, (2017). https://github.com/rclab-auth/gidopensees.

[17] CIMNE, GiD, (2020). www.gidhome.com.

[18] C. Zhang, J.G. Silva, C. Weinschenk, D. Kamikawa, Y. Hasemi, Simulation Methodology for Coupled Fire-Structure Analysis: Modeling Localized Fire Tests on a Steel Column, Fire Technol. 52 (2016) 239–262. https://doi.org/10.1007/s10694-015-0495-9.

[19] J.C.G. Silva, A. Landesmann, F.L.B. Ribeiro, Fire-thermomechanical interface model for performance-based analysis of structures exposed to fire, Fire Saf. J. 83 (2016) 66–78. https://doi.org/10.1016/j.firesaf.2016.04.007.

[20] K. Prasad, H.R. Baum, Coupled fire dynamics and thermal response of complex building structures, Proc. Combust. Inst. 30 (2005) 2255–2262. https://doi.org/10.1016/j.proci.2004.08.118.

[21] A.A. Khan, M.A. Khan, A. Usmani, X. Huang, S. Bakhtiyari, M.J. Ashtiani, S. Garivani, A.A.

Aghakouchak, Framework for Fire Investigation of Tall Buildings: A Case Study of the Plasco Building, Fire Technol. (2021). In press.

[22] D. Woo, J.K. Seo, Numerical validation of the two-way fluid-structure interaction method for non-linear structural analysis under fire conditions, J. Mar. Sci. Eng. 9 (2021). https://doi.org/10.3390/jmse9040400.

[23] A.A. Khan, M.A. Khan, C. Zhang, L. Jiang, A. Usmani, OpenFIRE: An Open Computational Framework for Structural Response to Real Fires, Fire Technol. (2021). In press.

[24] P. Bernardi, E. Michelini, A. Sirico, S. Rainieri, C. Corradi, Simulation methodology for the assessment of the structural safety of concrete tunnel linings based on CFD fire – FE thermo-mechanical analysis: a case study, Eng. Struct. 225 (2020). https://doi.org/10.1016/j.engstruct.2020.111193.

[25] K. Bergmeister, P. Brunello, M. Pachera, F. Pesavento, B.A. Schrefler, Simulation of fire and structural response in the Brenner Base Tunnel by means of a combined approach: A case study, Eng. Struct. 211 (2020). https://doi.org/10.1016/j.engstruct.2020.110319.

[26] J.A. Feenstra, H. Hofmeyer, R.A.P. Van Herpen, M. Mahendran, Automated two-way coupling of CFD fire simulations to thermomechanical FE analyses at the overall structural level, Fire Saf. J. 96 (2018) 165–175. https://doi.org/10.1016/j.firesaf.2017.11.007.

[27] M.A. Orabi, OpenSees for Fire: ISE, (2021). https://github.com/Anwar8/MyOpenSees.

[28] M.A. Orabi, GiD + OpenSees Thermo-mechanical Interface, (2021). https://github.com/Anwar8/gidopensees.

[29] L. Jiang, M.A. Orabi, J. Jiang, A. Usmani, Modelling concrete slabs subjected to fires using nonlinear layered shell elements and concrete damage-plasticity material, Eng. Struct. 234 (2021) 111977. https://doi.org/10.1016/j.engstruct.2021.111977.

[30] M.A. Orabi, L. Jiang, Q. Jin, A. Usmani, Modelling concrete slabs subjected to localised fire action with OpenSees, J. Struct. Fire Eng. (2021). In press.

[31] J. Lee, G.L. Fenves, Plastic-damage model for cyclic loading of concrete structures, J. Eng. Mech. 124 (1998) 892–900. https://doi.org/10.1061/(ASCE)0733-9399(1998)124:8(892).

[32] J. Lee, G.L. Fenves, A return-mapping algorithm for plastic-damage models: 3-D and plane stress formulation, Int. J. Numer. Methods Eng. 50 (2001) 487–506. https://doi.org/10.1002/1097-0207(20010120)50:2%3C487::AID-NME44%3E3.0.CO;2-N.

[33] A. Usmani, J. Zhang, J. Jiang, Y. Jiang, I. May, Using Opensees for Structures in Fire, J. Struct. Fire Eng. 3 (2012) 57–70. https://doi.org/10.1260/2040-2317.3.1.57.

[34] X. Lu, L. Xie, H. Guan, Y. Huang, X. Lu, A shear wall element for nonlinear seismic analysis of super-tall buildings using OpenSees, Finite Elem. Anal. Des. 98 (2015) 14–25. https://doi.org/10.1016/j.finel.2015.01.006.

[35] X. Lu, Y. Tian, S. Cen, H. Guan, L. Xie, L. Wang, A High-Performance Quadrilateral Flat Shell Element for Seismic Collapse Simulation of Tall Buildings and Its Implementation in OpenSees, J. Earthq. Eng. 22 (2018) 1662–1682. https://doi.org/10.1080/13632469.2017.1297269.

[36] L. Jiang, S. Chen, A. Usmani, Feasibility of dimensionally reduced heat transfer analysis for structural members subjected to localised fire, Adv. Struct. Eng. 21 (2018) 1708–1722. https://doi.org/10.1177/1369433218754334.

[37] V.K.R. Kodur, A.M. Shakya, Effect of temperature on thermal properties of spray applied fire resistive materials, Fire Saf. J. 61 (2013) 314–323. https://doi.org/10.1016/j.firesaf.2013.09.011.

[38] Q. Li, C. Zhang, G.Q. Li, Symmetric modeling of the thermal actions in a structural fire experiment on a

long-span composite floor beam in a compartment, Fire Saf. J. 120 (2021) 103079. https://doi.org/10.1016/j.firesaf.2020.103079.

[39] L. Choe, S. Ramesh, L. Choe, M. Seif, Compartment Fire Experiments on Long-Span Composite-Beams with Simple Shear Connections Part 1 : Experimental Design and Beam Behavior at Ambient Temperature NIST Technical Note 2054 Compartment Fire Experiments on Long-Span Composite-Beams with Simple Sh, 2019. https://www.nist.gov/publications/compartment-fire-experiments-long-span-composite-beams-simple-shear-connections-part-1.

[40] BSi, EN 1992-1-1:2004 Eurocode 2 — Design of concrete structures Part 1-1: General rules and rules for buildings, (2004).

[41] BSi, EN 1993-1-2:2005 Eurocode 3 — Design of Steel Structures Part 1-2: General rules — structural fire design, Br. Stand. (2006).

[42] K. McGrattan, S. Hostikka, R. McDermott, J. Floyd, C. Weinschenk, K. Overhold, Sixth Edition Fire Dynamics Simulator User 's Guide (FDS), NIST Spec. Publ. 1019. Sixth Edit (2016). https://doi.org/10.6028/NIST.SP.1019.

[43] NIST, NIST NCSTAR 1: Final Report on the Collapse of the World Trade Centre Towers, 2005. https://doi.org/10.6028/NIST.ncstar.1.

[44] M.A. Orabi, L. Jiang, A. Usmani, J. Torero, The Collapse of World Trade Center 7: Revisited, in: 11th Int. Conf. Struct. Fire, 2020: pp. 23–33.

[45] B. Merci, T. Beji, Fluid Mechanics Aspects of Fire and Smoke Dynamics in Enclosures, 1st ed., CRC Press, Leiden, 2016.

[46] H.R. Baum, M. K.B., R.G. Rehm, Three dimensional simulations of fire plume., in: Fire Saf. Sci. Proc.

Fifth Int. Symp., Tsukuba, Japan, 1997: pp. 511–522.

[47] T.G. Ma, J.G. Quintiere, Numerical simulation of axi-symmetric fire plumes: Accuracy and limitations, Fire Saf. J. 38 (2003) 467–492. https://doi.org/10.1016/S0379-7112(02)00082-6.

[48] G. Rein, J.L. Torero, W. Jahn, J. Stern-Gottfried, N.L. Ryder, S. Desanghere, M. Lázaro, F. Mowrer, A. Coles, D. Joyeux, D. Alvear, J.A. Capote, A. Jowsey, C. Abecassis-Empis, P. Reszka, Round-robin study of a priori modelling predictions of the Dalmarnock Fire Test One, Fire Saf. J. 44 (2009) 590–602. https://doi.org/10.1016/j.firesaf.2008.12.008.

[49] A. Alikhan, FDS2OpenSEES, (2021). https://github.com/aatif85/FDS2OpenSEES.

[50] A. Jowsey, Fire Imposed Heat Fluxes for Structural Analysis, The University of Edinburgh, 2006.

[51] BSi, EN 1991-1-2:2002: Eurocode 1: Actions on Structures — General actions-actions on structures exposed to fire, (2002).

[52] P.J. Moss, G.C. Clifton, Modelling of the cardington LBTF steel frame building fire tests, Fire Mater. 28 (2004) 177–198. https://doi.org/10.1002/fam.868.

[53] Z. Huang, I.W. Burgess, R.J. Plank, Three-dimensional modelling of two full-scale fire tests on a composite building, Proc. Inst. Civ. Eng. - Struct. Build. 134 (1999) 243–255. https://doi.org/10.1680/istbu.1999.31567.

[54] SFPE, SFPE Handbook of Fire Protection Engineering, 2016. https://doi.org/10.1016/s0379-7112(97)00022-2.

[55] J.G. Quintiere, Fundamental of Fire Phenomena, John Wiley, New York, 2006. https://doi.org/10.1002/0470091150.

[56] A.Y. Elghazouli, B.A. Izzuddin, Realistic Modeling of Composite and Reinforced Concrete Floor Slabs

under Extreme Loading. II: Verification and Application, J. Struct. Eng. 9445 (2004) 1562–1569. https://doi.org/10.1061/(ASCE)0733-9445(2004)130.

[57] X. Yu, Z. Huang, I. Burgess, R. Plank, Nonlinear analysis of orthotropic composite slabs in fire, Eng. Struct. 30 (2008) 67–80. https://doi.org/10.1016/j.engstruct.2007.02.013.

[58] P. Kotsovinos, A. Usmani, The World Trade Center 9/11 Disaster and Progressive Collapse of Tall Buildings, Fire Technol. 49 (2013) 741–765. https://doi.org/10.1007/s10694-012-0283-8.

[59] M. Gillie, A. Usmani, M. Rotter, M. O'Connor, Modelling of heated composite floor slabs with reference to the Cardington experiments, Fire Saf. J. 36 (2001) 745–767. https://doi.org/10.1016/S0379-7112(01)00038-8.

[60] X. Yu, Z. Huang, An embedded FE model for modelling reinforced concrete slabs in fire, Eng. Struct. 30 (2008) 3228–3238. https://doi.org/10.1016/j.engstruct.2008.05.004.

[61] K. McGrattan, S. Hostikka, J. Floyd, R. McDermott, K.J. Overholt, Fire Dynamics Simulator, Technical Reference Guide, 6th Ed., National Institute of Standards and Technology, 2019. https://www.nist.gov/publications/fire-dynamics-simulator-technical-reference-guide-sixth-edition.

[62] A.K. Abu, I.W. Burgess, R.J. Plank, Tensile membrane action of thin slabs exposed to thermal gradients, J. Eng. Mech. 139 (2013) 1497–1507. https://doi.org/10.1061/(ASCE)EM.1943-7889.0000597.

[63] S. Lamont, A.S. Usmani, M. Gillie, Behaviour of a small composite steel frame structure in a "long-cool" and a "short-hot" fire, Fire Saf. J. 39 (2004) 327–357. https://doi.org/10.1016/j.firesaf.2004.01.002.

[64] A.M. Sanad, J.M. Rotter, A.S. Usmani, M.A. O'Connor, Composite beams in large buildings under fire - Numerical modelling and structural behaviour, Fire Saf. J. 35 (2000) 165–188. https://doi.org/10.1016/S0379-7112(00)00034-5.

[65] E.I. Wellman, A.H. Varma, R. Fike, V. Kodur, Experimental evaluation of thin composite floor assemblies under fire loading, J. Struct. Eng. 137 (2011) 1002–1016. https://doi.org/10.1061/(ASCE)ST.1943-541X.0000451.

[66] A.S. Usmani, N.J.K. Cameron, Limit capacity of laterally restrained reinforced concrete floor slabs in fire, Cem. Concr. Compos. 26 (2004) 127–140. https://doi.org/10.1016/S0958-9465(03)00090-8.

[67] O. Vassart, B. Zhao, FRACOF: Fire Resistance Assessment of Partially Protected Composite Floors - Engineering Background, 2011.

[68] Z.N. Yang, Y.L. Dong, W.J. Xu, Fire tests on two-way concrete slabs in a full-scale multi-storey steel-framed building, Fire Saf. J. 58 (2013) 38–48. https://doi.org/10.1016/j.firesaf.2013.01.023.